Characterization and evolutionary inference of cold-shock domain proteins enhancing the reprogramming of differentiated gametophore leaf cells to chloronema apical stem cells in the moss *Physcomitrella patens*

Li, Chen

Doctor of Philosophy

Department of Basic Biology
School of Life Science
SOKENDAI (The Graduate University for Advanced Studies)

Characterization and evolutionary inference of cold-shock domain proteins enhancing the reprogramming of differentiated gametophore leaf cells to chloronema apical stem cells in the moss *Physcomitrella patens*

Li, Chen

PhD Dissertation

2017

TABLE OF CONTENTS

LIST OF FIGURES

LIST OF TABLE

ABSTRACT

Both plants and animals have the capacity to reprogram differentiated cells to stem cells. Multicellularity with stem-cell systems has evolved independently in land plant and metazoan lineages and the molecular mechanisms underlying reprogramming appear to differ between these lineages. Although several factors involved in reprogramming have been reported within each lineage (reviewed in [1-4]), no common factor has been identified between them. Here, the moss *Physcomitrella patens* (Physcomitrella) Cold-Shock Domain Protein 1 (PpCSP1), which shares highest amino-acid sequence similarity and the domain structure with the induced pluripotent stem cell (iPSC) factor Lin28 in mammals [5], was identified to regulate reprogramming of differentiated leaf cells to chloronema apical stem cells. PpCSP1 accumulated in the reprogramming cells and was maintained throughout the reprogramming process and in the resultant stem cells. Expression of *PpCSP1* was negatively regulated by its 3' untranslated region (UTR). Removal of the 3' UTR stabilized *PpCSP1* transcripts, resulting in elevated levels of *PpCSP1* transcripts and protein, as well as enhanced reprogramming. A quadruple deletion mutant of *PpCSP1* and three closely related *PpCSP* genes exhibited attenuated reprogramming, indicating that the *PpCSP* genes function redundantly in the cellular reprogramming. Taken together, these data demonstrate a positive role of PpCSP1 in reprogramming, which is similar to the function of mammalian Lin28.

1. GENERAL INTRODUCTION

Reprogramming in land plants and metazoa

Stem cells self-renew and produce cells to be differentiated during the development [1-4]. Although multicellularity and stem-cell systems arose independently in land plant and metazoan lineages, similarities exist in the mechanism of stem-cell formation and maintenance in both plant and animal kingdoms [2-4]. For example, stem cells are maintained by a group of cells known as a stem-cell niche. The homeostasis of stem-cell niche is critical for the self-renewal of stem cells and cell differentiation to new tissues and organs [1]. In addition, differentiated cells can change their cell fate to stem cells under certain conditions in both land plants and metazoa [3, 4].

In metazoa, there are many model systems for regeneration studies, such as the injured tail and limb of amphibians, the entire body of planarians and hydra, germ cells of Drosophila, and skin and gut in mice [6]. At the wounding site, a group of progenitor cells are formed, called blastema, which develop into whole organs or tissues [4]. Generally, regeneration can be divided into several types. The first example is the regeneration and restoration of the tissue which has same identity as that in the injured tissue, such as amphibian limb and tail regeneration [3, 4]. The second example is the regeneration of new type of tissues, the large parts of which do not exist at the injured site, such as whole body

regeneration in planarian and hydra after the dissection [3, 4]. However, in most of those cases, regeneration involves the activation or movement of existing undifferentiated cells, but not the reprogramming from differentiated cells to stem cells. For cellular reprogramming, a striking work was performed that nucleus-removed oocytes transplanted with the nucleus from intestine cells of an adult frog could successfully produce somatic nucleus-derived adult frogs [7]. This demonstrated that differentiated nuclei can be reprogrammed to become pluripotent by somatic cell nuclear transfer. The cellular reprogramming could be also derived by fusion of embryonal carcinoma cells with somatic cells. Thus, the resulting hybrid cells acquired similar features of embryonal carcinoma cells [8]. The outstanding breakthrough was the finding of induced pluripotent stem cell (iPSC). Prior to the iPSC finding, the induction of cellular reprograming had been accomplished as the induction of single transcription factor MyoD1 in various types of cells such as fibroblast, pigment, nerve, fat, and liver cells was sufficient to activate myogenesis pathway to convert them to myogenic cells [9, 10]. After this finding, iPSC was discovered that the induction of four factors is sufficient to reprogram somatic cells to pluripotent stem cells. Oct4, Sox2, cMyc, and Klf4 were first reported as iPSC factors able to reprogram mouse fibroblast cells into pluripotent stem cells [11]. Later, the same factors were applied to human fibroblast cells to be iPSCs [12]. At the same time, another set of pluripotency factors Oct4, Sox2, Nanog, and

Lin28 was identified, which can successfully induce pluripotent stem cells from human fibroblast cells [5]. The finding of iPSCs was the first time to prove that intact differentiated somatic cells could be reprogrammed to pluripotent stem cells in mammals.

In flowering plants, the reprogramming ability to stem cells is basically stronger than that in metazoa. In the model seed plant *Arabidopsis thaliana* (Arabidopsis), stem cells exist in the shoot apical meristem (SAM) and root apical meristem (RAM) and their self-renewal, differentiation, and patterning are well defined and characterized. SAM and RAM share similar pattern of stem cell regulation and contain stem cell niches with low mitotic activity cells, called as the central zone and the quiescent center [13-15]. These stem cell niches maintain the meristems that give rise to entire shoot and root, which contribute to the plant growth. It's well studied that CLAVATA-WUSCHEL pathway and PLETHORA-SHORT ROOT-SCARECROW transcription network play key roles in SAM and RAM maintenances and patterning [13-15]. Interestingly, a study of root regeneration in Arabidopsis showed that stem cell niche is not required for organ regeneration. This indicates that adult cells intrinsically bear the potency of cellular reprogramming to switch the cell fate upon injury [16].

On the other side, differentiated cells can form an undifferentiated cell mass, called callus, which regenerates shoot and root meristems including stem cells with appropriate

phytohormones. Such somatic embryogenesis was first established in carrot where a root derived cell can regenerate a whole plant though the callus [17]. This classical finding inferred that plant cells have an ability to be reprogrammed into the totipotent state under certain conditions. In Arabidopsis, the callus formed on the auxin- and cytokinin-containing medium is not a mass of unorganized cells but consists of the cells with the identity of lateral root primordia [18]. This was further confirmed by transcriptome analysis as callus has more similar expression profile to root meristem tissues than shoot meristem or embryonic tissues [18]. Several genes have been characterized to be involved in the formation of callus or stem cells in Arabidopsis [19]. LATERAL ORGAN BOUNDARIES DOMAIN (LBD) family transcription factors, including LBD16, LBD17, LBD18, and LBD29 were upregulated by auxin which is a strong inducer of lateral root formation in Arabidopsis [20]. Overexpression of each of these four LBD genes was sufficient to induce callus formation without exogenous hormones via AUXIN RESPONSE FACTOR7 (ARF7) and ARF19 pathway [20]. Wounding induces callus formation in Arabidopsis seedlings, in which the molecular mechanism differs from that in callus induction by hormone treatments. Wounding induces the expression of a plant-specific AP2/ERF transcription factor gene *WOUND INDUCED DEDIFFERENTIATION 1* (*WIND1*), and overexpression of *WIND1* enhances callus formation without exogenous hormones [21]. Overexpression of another AP2/ERF

transcription factor ENHANCER OF SHOOT REGENERATION 1 (ESR1)/DORNROESCHEN (DRN) promotes the formation of shoot meristems from the callus [22].

So far, except for one example, genes involved in stem-cell formation and maintenance are specific in land plant- or metazoan lineage, despite the similarities in the stem-cell systems such as a stem-cell niche in both kingdoms [2]. At present, the RETINOBLASTOMA-RELATED protein is the only known common factor involved in stem cell function in both land plant and metazoan kingdoms, however, no common factor involved in the reprogramming from differentiated cells to stem cells have been identified [2, 23]. This is not surprising, because land plants and metazoa had diverged at the unicellular stage and the stem-cell systems evolved independently in their lineages. It is still unknown whether land plants and metazoa use any similar mechanisms for the reprogramming from differentiated cells to stem cells. The researches to compare the stem-cell system and reprogramming between land plant and metazoan lineages will provide critical insights into the principles and mechanisms of reprogramming during the evolution. In this study, a bryophyte, *Physcomitrella patens* (Physcomitrella), in which differentiated cells have a remarkable ability of being reprogrammed into stem cells without callus formation, was chosen to investigate the reprogramming in land plants.

2. EVOLUTIONARILY RELATED COLD-SHOCK DOMAIN PROTEINS REPROGRAM DIFFERENTIATED CELLS TO STEM CELLS IN LAND PLANTS AND METAZOA

2.1 INTRODUCTION

2.1.1 The moss *Physcomitrella patens* as an model plant for stem-cell researches

Physcomitrella is an excellent model plant with many advantages [24]. It is the first bryophyte with the sequenced genome and a nice model for evolutionary and developmental studies [25]. Physcomitrella has a high efficiency for gene targeting via homologous recombination that enables reverse genetics approach to investigate gene function [26, 27]. Moreover, it is also an useful plant for stem-cell studies [28]. Physcomitrella has dominant haploid generation and a simple stem cell system. After spore germination, a chloronema apical stem cell shows tip growth and continually produces chloronema cells by asymmetric cell divisions, which forms filamentous tissues named protonemata. A chloronema apical stem cell divides to regenerate itself and form a chloronema subapical cell that fulfill the definition of stem cell: they self-renew and give rise to cells that go on to differentiate [28]. Gametophores are shoots with single cell-layer leaves, and are formed from protonemata in the haploid generation. When a differentiated leaf is excised from the gametophore and cultivated on a medium without phytohormones, leaf cells facing the cut change to chloronema apical stem cells with tip growth and then divide approximately 30 hours after excision (Figure 1) [28, 29]. The transition of

differentiated leaf cells to chloronema apical stem cells enables researchers to investigate the reprogramming process at the cellular level.

To understand the molecular mechanisms of the reprogramming, these underlying the stem-cell formation of Physcomitrella have been investigated. Transcriptome analysis was performed during the reprogramming [30] and several key factors have been identified to play significant roles in the processes. For instance, Cyclin-Dependent Kinase A (CDKA) activation is essential for cell cycle progression during the reprograming [29]. *WUSCHEL-related homeobox 13-like* (*WOX13L*) genes are required for the initiation of tip growth during stem-cell formation [31].

2.1.2 Functions of cold-shock domain proteins and Lin28 in land plants and metazoa

In this study, Physcomitrella cold-shock domain proteins, which share highest sequence similarity and domain structure with Lin28 in metazoa, were identified to be involved in the reprogramming in the land plant.

The Cold Shock Domain (CSD) was first identified in bacteria as proteins expressed under cold shock conditions [32], and were later implicated in the process of cold acclimation in flowering plants as CSP transcripts accumulate after cold treatment in Arabidopsis and wheat [33-35]. CSD possesses the nucleic acid-binding activity and is

capable to bind to single-stranded DNA/RNA and double-stranded DNA [36]. CSD is highly conserved in bacteria, land plants and metazoa, although most land plant CSPs and some metazoan CSPs bear CCHC zinc-finger domains but bacteria CSPs do not [37, 38]. In *Escherichia coli*, CSPs function as RNA chaperones that destabilize secondary structures in RNAs and deletion of four CSP genes results in growth defect under low temperature [39, 40]. Wheat cold-shock domain protein 1 (WCSP1) was the first analyzed CSP protein in land plants, which also accumulates during cold acclimation. WCSP1 also has nucleic acid binding activity, antitermination activity and dsDNA melting activity. Ectopic expression of WCSP1 in *Escherichia coli* CSPs deletion mutant could complement its cold-sensitive phenotype, suggested a conserved function of CSP in bacteria and land plants [35]. The conserved function of CSP proteins was further confirmed by the study of Arabidopsis CSP proteins [33, 34].

Lin28 was first described in nematode *Caenorhabditis elegans* (*C. elegans*) as a heterochronic gene that affects the developmental timing [41]. Lin28 is a conserved RNA-binding protein with an N-terminal CSD and C-terminal CCHC zinc-finger domains. Loss-of-function on *Lin28* of the worm accelerates differentiation of hypodermal and vulval stem cells. In contrast, gain-of-function of *Lin28* promotes self-renew and delays the differentiation of hypodermal and vulval stem cells [42]. One heterochronic microRNA *let-7*

represses Lin28 post-transcriptionally through direct binding to the 3' UTR of Lin28 [43]. In mammalian cell systems, Lin28 is highly expressed in undifferentiated cells while *let-7* enriches in somatic cells [5]. Lin28 directly prevents the post-transcriptional maturation of *let-7,* which in turn represses Lin28 itself [44]. X-ray crystallography of Lin28-let-7 protein-RNA complex revealed that Lin28 binds to pre-let-7 at terminal loop and GGAG motif [45]. In addition to the stem-cell regulation, overexpression of Lin28, with a set of pluripotency associated transcription factors Oct4, Sox2 and Nanog, promotes reprogramming of human somatic fibroblasts into self-renewing iPSCs [5]. These results indicate that Lin28 plays a critical role in the self-renewal of pluripotent stem cells and that Lin28 and *let-7* constitute the bistable switch to control stem cell self-renewal [43]. Since Lin28 is an RNA-binding protein, several studies of genome-wide cross-linking immunoprecipitation sequencing (CLIP-seq) revealed that Lin28 binds to various mRNA with recognitions of GGAG or GGAG-like motif [46-48]. Further study by comparison of CLIP-seq with ribosome footprint sequencing indicates translation repression of certain target mRNAs designated at ER where translation occurs [46]. Ectopic expression of Lin28 can enhance tissue repair in mice through binding to mRNAs of several oxidative metabolic enzymes and promoting their translation, suggesting that metabolic networks mediated by Lin28 regulate stem-cell homeostasis [49].

In this study, the cold-shock domain protein PpCSP1, which shares highest amino-acid sequence similarity and domain structure with Lin28 in metazoa, was characterized and found to be involved in the enhancement of reprogramming in Physcomitrella. Investigation of the function of PpCSP1 may give insights into the evolution of reprogramming from differentiated cells to stem cells in land plant and metazoan lineages.

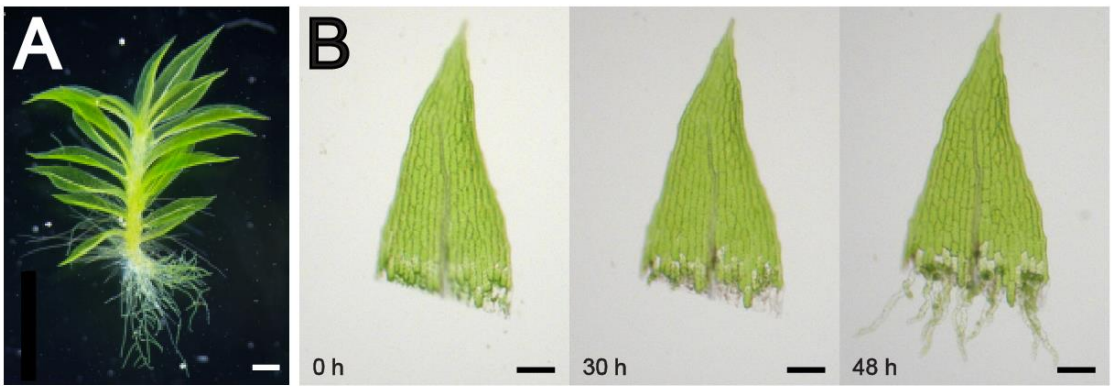

Figure 1. Reprogramming from differentiated cells to stem cells in Physcomitrella

(A) A wild-type gametophore 4 weeks after inoculation.

(B) A wild-type leaf at 0, 30, and 48 hours after excision.

Scale bars represent 500 µm in (A), 100 µm in (B).

2.2 MATERIALS AND METHODS

2.2.1 Plant material

The Gransden 2004 strain of *Physcomitrella patens* [25] was used as the wild-type strain and cultured on BCDAT medium under continuous white light at 25˚C [50]. The third or fourth leaves were excised from gametophores on a plate 3 weeks after inoculation and put into liquid BCDAT medium to induce the reprogramming [29]. Polyethylene glycol-mediated transformation and preparation of gametophores were performed as previously described [29, 50].

2.2.2 Accession numbers

Sequence data of *PpCSP*s can be found from Phytozome *Physcomitrella patens* V3.3 (http://phytozome.jgi.doe.gov/pz/portal.html#!info?alias=Org_Ppatens) under the following accession numbers: *PpCSP1* (Pp3c5_6070), *PpCSP2* (Pp3c6_23240), *PpCSP3* (Pp3c5_7920), and *PpCSP4* (Pp3c5_7880).

2.2.3 Plasmid construction for expression analysis

Primers used for plasmid construction are provided in Table 1. To insert the *Citrine* coding sequence (CDS) [51] in frame with the *PpCSP1* CDS, a *PpCSP1* genomic DNA fragment

just prior to the stop codon and a fragment just after the stop codon, were amplified and cloned into pCTRN-NPTII 2 (AB697058); thereby generating nPpCSP1-Citrine-nosT line (Figure 2). One microgram of circular Cre recombinase [52] expression plasmid (AB542060), as extracted from the *E.coli* DH5α strain with Wizard Plus SV Minipreps DNA Purification System kit (Promega) without any restriction enzyme digestion, was introduced into the PpCSP1-Citrine line to excise the selection marker cassette and the nopaline synthase terminator flanked by two loxP sites to generate the nPpCSP1-Citrine-3'UTR line. The regenerated lines were screened not grow on a medium containing 20 mg/L G418 and candidate lines were further confirmed by PCR.

For the promoter reporter lines, a 2.2-kb fragment containing a gateway rfcA cassette (Invitrogen) and a terminator sequence of pea (*Pisum sativum*) *rbcS3A* gene was amplified by PCR from the plasmid pT1OG (LC126301) with the primer pair shown in Table 1 and then transferred into the XbaI-HindIII cut pPIG1b-NGGII plasmid (AB537478), resulting in the plasmid pAK101. A luciferase coding sequence was amplified from pGL4.10 (Promega) and inserted into the StuI site of pAK101, resulting in a gateway-luciferase binary vector pAK102. A 1.8-kb PpCSP1 promoter fragment was amplified and cloned into the pENTR/D-TOPO vector (Invitrogen). The PpCSP1pro:LUC plasmid was constructed by LR reaction between the entry plasmid and pAK102. This construct was introduced to

nPpCSP1-Citrine-3'UTR line to generate the PpCSP1pro:LUC nPpCSP1-Citrine-3'UTR line (Figure 2C).

2.2.4 Plasmid construction of *PpCSP1* 3' UTR deletion series and transient expression of these constructs using particle bombardment

Primers used for plasmid construction are provided in Table 1. sGFP and mRFP were inserted into pTKM1 vector [53] to generate pTKM1-sGFP and pTKM1-mRFP vectors. Different lengths of the *PpCSP1* 3' UTR were amplified with wild-type genomic DNA as a template and inserted just after the sGFP coding sequence at the *Apa*I site (Figure 13A).

Sixty mg gold particles (1.6 μm diameter) were coated with equal quantities of each pair of pTKM1-mRFP/ pTKM1-sGFP plasmid DNA and bombarded by PDS-1000 (Bio-rad) under 94.5 KPa vacuum condition into 5-week old gametophores. Digital images were obtained using an Olympus DP71 camera on a fluorescence microscope (SZX16, Olympus, Japan). Fluorescence intensity of specific leaf cells was quantified by ImageJ 1.48v.

2.2.5 Plasmid construction for EF1αpro:sGFP-nosT and EF1αpro:sGFP-3'UTR lines

Primers used for plasmid construction are given in Table 1. Fragments of sGFP and sGFP-3'UTR were amplified from pTKM1-sGFP-3'UTR plasmid and cloned into

pENTR/D-TOPO (Invitrogen) and subsequently inserted into the pT1OG vector (LC126301) [54] (Figure 10).

2.2.6 Plasmid construction for the PpCSP1pro:PpCSP1-Citrine line

Primers used for plasmid construction are provided in Table 1. A fragment of 2.1-kb *PpCSP1* promoter and *PpCSP1* genic sequence without the stop codon was amplified from wild-type genomic DNA and inserted into pCTRN-NPTII with *Xho*I and *Bsr*GI sites. The fragment containing the *PpCSP1* promoter, PpCSP1-Citrine fusion gene and nptII cassette was subsequently digested by *Sma*I and inserted into the pPTA1 vector (LC122350) (which contains the targeting sequence to PTA1 locus [54]) to generate the PpCSP1pro:PpCSP1-Citrine line (Figure 16).

2.2.7 Plasmid construction for the deletion of *PpCSP* genes and generation of the *PpCSP*-deletion mutants

Primers used for plasmid construction are provided in Table 1. To delete *PpCSP1*, *PpCSP2*, *PpCSP3* and *PpCSP4* in wild-type Physcomitrella, genomic fragments containing the 5'- and 3'-flanking regions of each gene were inserted into the 5'-end and 3'-region of the nptII expression cassette of pTN182 (AB267706), of the hygromycin resistance cassette of

pTN186 (AB542059), of the BSD expression cassette of p35S-loxP-BSD (AB537973), and of the Zeocin resistance cassette of p35S-loxP-Zeo (AB540628) plasmids, respectively. The generated constructs were digested by suitable restriction enzymes for gene targeting (Figure 19).

To generate *ppcsp* quadruple deletion mutants, the *PpCSP1*-deletion construct was introduced into wild-type Physcomitrella to generate *ppcsp1* lines. The *PpCSP*2-deletion construct, *PpCSP*3-deletion construct, and subsequently the *PpCSP*4-deletion construct were introduced into the *ppcsp1* lines to generate the *ppcsp1 ppcsp2* double deletion mutants, *ppcsp1 ppcsp2 ppcsp3* triple deletion mutants, and *ppcsp1 ppcsp2 ppcsp3 ppcsp4* quadruple deletion mutants, respectively.

2.2.8 DNA gel blot analysis

DNA gel blot analysis was performed as below: Approximately 3 µg of genomic DNA was digested with appropriate restriction enzyme(s) (see Figures and the legends), run on 0.7% (w/v) SeaKemGTG agarose (BME, Rockland, ME, USA), and transferred to a Hybond N^+ nylon membrane (GE Healthcare, Chicago, IL, USA). Probe labeling, hybridization, and detection were performed using the AlkPhos direct labeling and detection system with

CDP-Star (GE Healthcare) according to the supplier's instructions. [29]. Primers used for probe amplification are provided in Table 1.

2.2.9 Phylogenetic analysis

Phylogenetic analysis with Neighbour-Joining method [55] was performed as described previously [56], with updated datasets [57] including sequences from *Klebsormidium flaccidum* [58]. The non-redundant (nr) dataset used was as of Jan 17, 2015.

BLASTP search against a dataset consisting of the nr as of Jan, 2015, Klebsormidium dataset from http://www.plantmorphogenesis.bio.titech.ac.jp/~algae_genome_project/klebsormidium/kf_download.htm *Pinus taeda* assembly 1.01 annotation v2 http://dendrome.ucdavis.edu/ftp/Genome_Data/genome/pinerefseq/Pita/v1.01/Pita_Annotation_v2/, and *Physcomitrella patens* v1.6 dataset https://www.cosmoss.org/physcome_project/linked_stuff/Annotation/V1.6/P.patens.V6_filtered_cosmoss_proteins.fas.gz, were performed using PpCSP1 through http://moss.nibb.ac.jp/cgi-bin/blast-nr-Kfl. Although Lin28 proteins share highest similarity with PpCSP1 in metazoan databases, the number of Lin28 proteins obtained from the BLASTP search was not so many, because many CSPs in land plants appeared before

Lin28 proteins. To obtain more Lin28 proteins, the BLASTP search was performed using *C. elegans* Lin28 as query. Top 700 for *PpCSP1* and 600 for Lin28 hit sequences were recovered and aligned through http://moss.nibb.ac.jp/cgi-bin/selectNalign and a preliminary tree was drawn with http://moss.nibb.ac.jp/cgi-bin/makenjtree. From both trees, sparse sampling of terminal taxa was performed. These sequences were further aligned using MAFFT [59] with the einsi option through http://moss.nibb.ac.jp/cgi-bin/selectNalign. Sites aligned ambiguously or having gaps were marked as excluded for further analysis using MacClade ver 4 [60]. The edited nexus format file was submitted from http://moss.nibb.ac.jp/cgi-bin/makenjtree to construct a NJ tree. The maximum likelihood distances under the JTT model were calculated using PROTDIST in PHYLIP package and a NJ tree was constructed [61].

After removing genes lacking conserved zinc-finger domains and marking those regions as included, the nexus file was submitted from http://moss.nibb.ac.jp/cgi-bin/makemltree1000. This selects an amino acid substitution model based on the data and performs maximum likelihood analysis using RAxML version 8.1.16. Bootstrap analysis was performed with 1000 replicates prepared with SEQBOOT in PHYLIP and consensus was calculated with CONSENSE [61, 62].

2.2.10 RNA preparation and RT-qPCR analysis

Total RNA was purified from protonemata and cut leaves with the RNeasy Micro Kit (Qiagen). First strand cDNA was synthesized using the ReverTra Ace qPCR RT Master Mix (TOYOBO). RT-qPCR was performed using an ABI PRISM 7500 (Applied Biosystems) with the QuantiTect SYBR Green PCR Kit (Qiagen). The cycle conditions were: 50°C for 2 min and 95°C for 10 min as pre-treatments, 95°C for 15 sec and 60°C for 1 min at 40 cycles as amplification. After amplification cycles, I carried out dissociation analyses for confirmation of target validity. The sequences of primers for RT-qPCR are listed in Table 1. Standard curves were estimated by dilution series (1, 0.1, 0.01, 0.001 and 0.0001) of one wild-type cDNA sample. Each transcript level determined by RT-qPCR analysis was normalized with *TUA1* [29].

2.2.11 Digital gene expression profiling with mRNA 5'-end tags (5'-DGE) analysis

Transcriptome comparisons between the nPpCSP1-Citrine-nosT line and the nPpCSP1-Citrine-3'UTR line were performed as previously described [30] (DRA accession number DRR055536-DRR055559). From 5 to 10 μg of total RNA, poly(A) RNA was enriched with the FastTrack Kit (Thermo Fisher Scientific, Waltham, MA). Then, first-strand cDNA was synthesized using biotin-labeled dT20 primers containing an EcoP15I site

(Biotin-TEG-5’-CTATCAGCAGTTTTTTTTTTTTTTTTTTT-3’) using PrimeScript II reverse transcriptase (Takara Bio, Shiga, Japan). DNA synthesis extended after the 5’ end of the mRNA, complementary to the biotin-labeled P2 DNA-RNA chimeric oligonucleotide containing an EcoP15I site and a GGG ribonucleotide sequence (Biotin-TEG-5’-CTGCCCCGGGTTCCTCATTCTCTCAGCArGrGrG-3’). The second-strand cDNA was synthesized based on the P2 sequence. After digestion with EcoP15I, the fragments were captured with streptavidin beads and ligated with P1 adaptors which were produced by annealing P1-A (5’-CCACTACGCCTCCGCTTTCCTCTCTATGGGCAGTCGGTGAT-3’) and P1-B-NN oligonucleotides (5’-N*N*ATCACCGACTGCCCATAGAGAGGAAAGCGGAGGCGTAGTGG-3’, where asterisks indicate phosphorothioate bonds). The resulting 25-bp 5’ cDNA fragments were amplified by 12 cycles of PCR using P1 (5-CCACTACGCCTCCGCTTTCCTCTCTAT-3’) and P2 primers (5’-CTGCCCCGGGTTCCTCATTCT-3’) and were then subject to 25-bp SOLiD single-read sequencing from the P1 sites. For the comparison between nPpCSP1-Citrine-nosT and nPpCSP1-Citrine-3’UTR lines, special reference for each line with the targeted change on the scaffold_41 where the *PpCSP1* locus is present was prepared and the sequence tags were mapped on the respective reference. Expression

profiles of gametophore leaves 0, 1, 3 and 6 hours after excision in nPpCSP1-Citrine-nosT lines, nPpCSP1-Citrine-3'UTR lines and wild type [31] were analyzed. Cumulative sum of tags of *PpCSP1* transcript for all time points in these lines were calculated and shown in Figure 9.

2.2.12 Microscopy and image analyses

Live imaging analysis was performed using a fluorescence microscope (IX81, Olympus) with a cooled CCD camera (ORCA-AG, Hamamatsu Photonics) or an EM-CCD camera (ImagEM, Hamamatsu Photonics). For luciferase bioluminescence imaging, tissues were pre-cultured for 18 hours in BCDAT medium, including 500 µM beetle luciferin potassium salt (Promega), prior to the observation. The third or fourth leaves were excised from gametophores on a plate 3 weeks after inoculation and placed on a 35 mm glass-based dish (IWAKI) covered with 2% methylcellulose. The leaves were covered with cellophane and then with 0.8% solid BCDAT medium. The petri dish was set on the stage of an IX81 microscope. Bright-field and Citrine-fluorescence images (using the 10x objective lens) of excised leaves were taken at 20-min intervals for 72 hours after excision. A U-MNIBA3 filter (Olympus) was used for Citrine. For the bioluminescence imaging with the time-lapse observation, images were taken at 2-hour intervals for 72 hours after the excision. A

U-MGFPHQ filter (Olympus) was used for the detection. Between imaging, the stage was moved in continuous white light conditions under control of the MetaMorph software (Molecular Devices). The area and intensity of the Citrine, luciferase or sGFP signal in each cell were calculated. The average intensity at each time point was calculated as the intensity of the GFP signal divided by the area of the cell. The movie of the time-lapse images was edited with ImageJ 1.48v. Images of PpCSP1-Citrine localization (Figure 5C) were taken by an inverted microscope (IX81, Olympus) equipped with a spinning-disk unit (CSU21, Yokogawa) with a CMOS camera (ORCA-Flash 4.0, Hamamatsu Photonics). Bandpass filters (FF01-550/88-25, Semrock) for Citrine were used in the spinning-disk unit. Gametophore apex images (Figure 5D) were taken by a fluorescence microscope (BX51, Olympus) equipped with a color camera (DS-Fi1c, Nikon). Citrine fluorescence images were taken with U-MNIBA3 filter (Olympus). Aphidicolin treatment [29] was performed as excised leaves were put into BCDAT liquid medium containing aphidicolin at the concentration denoted in Figure 22 or mock (DMSO). The leaves 72 h or 120 h after excision were stained in a solution containing 0.1% aniline blue and 0.1% K_3PO_4 (pH 12.5) to visualize newly synthesized cell plates. Fluorescent images were taken by a fluorescence microscope (BX51, Olympus) equipped with a color camera (DS-Fi1c, Nikon) and with long pass filter (U-MWU2, Olympus) (Figure 22). Protonema and gametophore images of

EF1αpro:sGFP-nosT and EF1αpro:sGFP-3'UTR lines (Figures 11E and 11F) and bombardment experiment images (Figure 13B) were taken by a fluorescence microscope (SZX16, Olympus) equipped with a color camera (DP71, Olympus). sGFP fluorescence was taken by GFPHQ filter (Olympus). mRFP fluorescence was taken by an RFP1 filter (Olympus) for excitation and 593/40 filter (Semrock) for emission. Fluorescence linearity of the color camera DP71 was examined with fluorescence beads. Images showing a fluorescence intensity that fitted within the linear range were chosen for quantitative analysis.

2.2.13 *In vivo* RNA binding assay

Cross-linking immunoprecipitation (CLIP) was performed as described before with modifications [63, 64]. One-week old protonema tissues of nPpCSP1-Citrine-3'UTR #1 and EF1αpro:Citrine #1 lines were rinsed in ice-cold PBS buffer and irradiated twice with 200 mJ/cm^2 UV. After UV irradiation, protonema tissues were lysed and subsequently immunoprecipitated using anti-GFP antibody (ab280; Abcam) to purify cross-linked RNA-protein complexes. The RNA-protein complexes were completely digested by micrococcal nuclease (Fermentas) at 10^{-3} dilution and treated with T4 PNK enzyme (Fermentas) and ^{32}P -γ-ATP to label RNA-protein complexes. Proteins and RNAs signals

were obtained by immunoblot analysis and autoradiography, respectively.

2.3 RESULTS

2.3.1 PpCSP1 shares conserved domains with Lin28

CSPs were first identified in bacteria as proteins expressed under cold shock conditions [32], and were later implicated in the process of cold acclimation in plants as CSP transcripts accumulate after cold treatment in Arabidopsis and wheat [33-35]. To better understand the evolution of CSPs, the function of the *PpCSP1* gene in Physcomitrella was investigated since no previous study had focused on CSPs in non-flowering plants [37]. To characterize the expression pattern of PpCSP1, a PpCSP1-Citrine fusion protein (nPpCSP1-Citrine-nosT line; Figures 2A and 2B) was generated. Using live imaging, predominant PpCSP1-Citrine signals were detected in chloronema and caulonema apical stem cells, which self-renew and produce cells that differentiate into chloronema and caulonema cells, respectively (Figure 3). The signals were also detected in chloronema and caulonema side branch initial cells, which are typically destined to become chloronema apical stem cells (Figure 3). These results suggested the possible involvement of PpCSP1 in stem cell maintenance and in the reprogramming of differentiated chloronema and caulonema cells to chloronema apical stem cells [28]. PpCSP1 contains a Cold Shock Domain (CSD), which is capable of binding to single-stranded DNA and RNA as well as to double-stranded DNA [36]. In addition, a search for conserved domains [65]

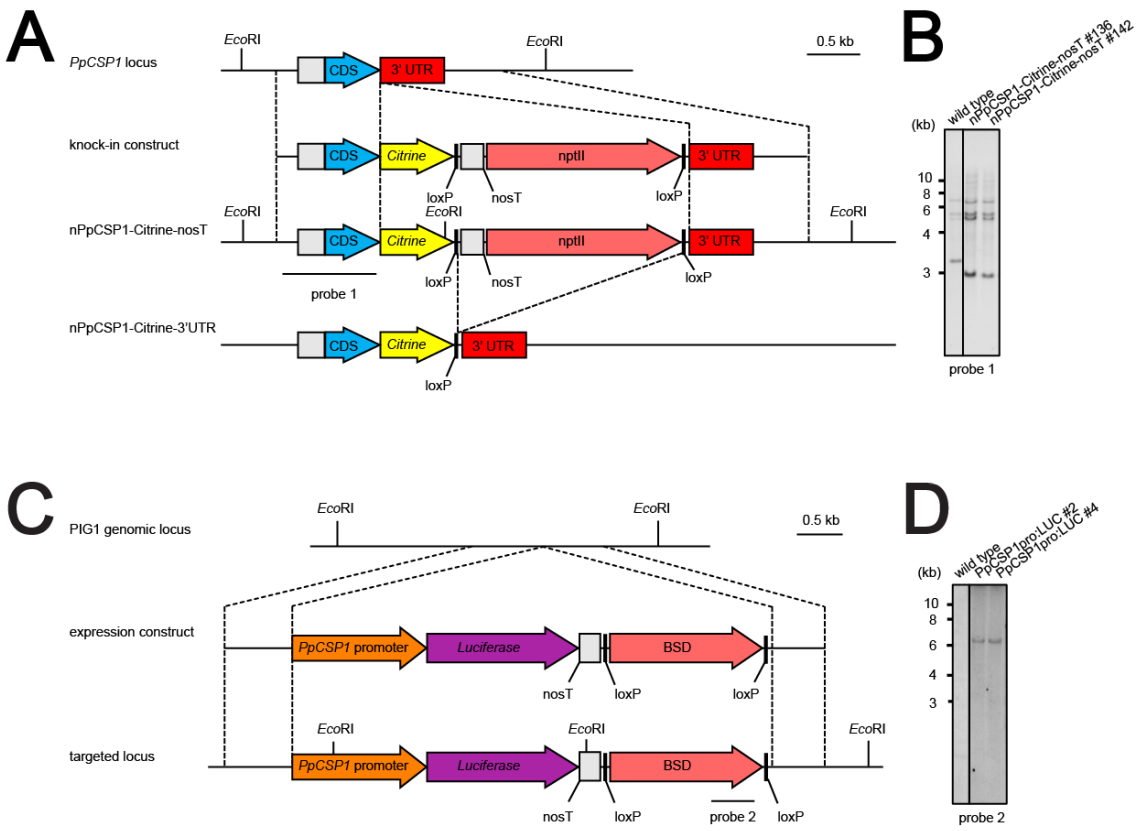
A
PpCSP1 locus
knock-in construct
nPpCSP1-Citrine-nosT
nPpCSP1-Citrine-3'UTR
EcoRI
CDS
3' UTR
Citrine
nptII
loxP
nosT
probe 1
0.5 kb
B
wild type
nPpCSP1-Citrine-nosT #136
nPpCSP1-Citrine-nosT #142
(kb)
10
8
6
4
3
probe 1
C
PIG1 genomic locus
expression construct
targeted locus
PpCSP1 promoter
Luciferase
BSD
probe 2
D
wild type
PpCSP1pro:LUC #2
PpCSP1pro:LUC #4
(kb)
10
8
6
4
3
probe 2

Figure 2. Construction of the nPpCSP1-Citrine-nosT, nPpCSP1-Citrine-3'UTR, and PpCSP1pro:LUC nPpCSP1-Citrine-3'UTR lines

(A) Schematic showing the insertion of a Citrine expression construct into the *PpCSP1* locus and removal of the nopaline synthase polyadenylation signal (nosT) and neomycin phosphotransferase II expression cassette (nptII) [50]. Blue, yellow, and pink arrows represent the *PpCSP1* coding sequence (CDS), *Citrine* CDS [51], and the nptII expression cassette, respectively. Gray and red boxes denote nosT [29] and 3' UTR of *PpCSP1*, respectively. The probe used in (B) is indicated. The nosT and nptII expression cassette were removed from the genome by transiently introducing plasmid DNA encoding Cre enzyme to produce nPpCSP1-Citrine-3'UTR lines (bottom).
(B) DNA gel-blot analysis of targeted lines. Genomic DNA of wild type and nPpCSP1-Citrine-nosT (#136 and #142) lines was digested with *Eco*RI.
(C) Schematic showing the insertion of the PpCSP1pro:LUC construct into the PIG1 locus [53, 66] in nPpCSP1-Citrine-3'UTR background. Orange, purple, and pink arrows denote the *PpCSP1* promoter, the DNA fragment encoding luciferase protein, and the blasticidin S deaminase expression cassette (BSD) [29], respectively. Gray and black boxes denote the nosT and the loxP [52] sequence, respectively. The probe used in (D) is indicated.
(D) DNA gel-blot analysis of targeted lines. Genomic DNA of wild type and PpCSP1pro:LUC (#2 and #4) lines was digested with *Eco*RI.

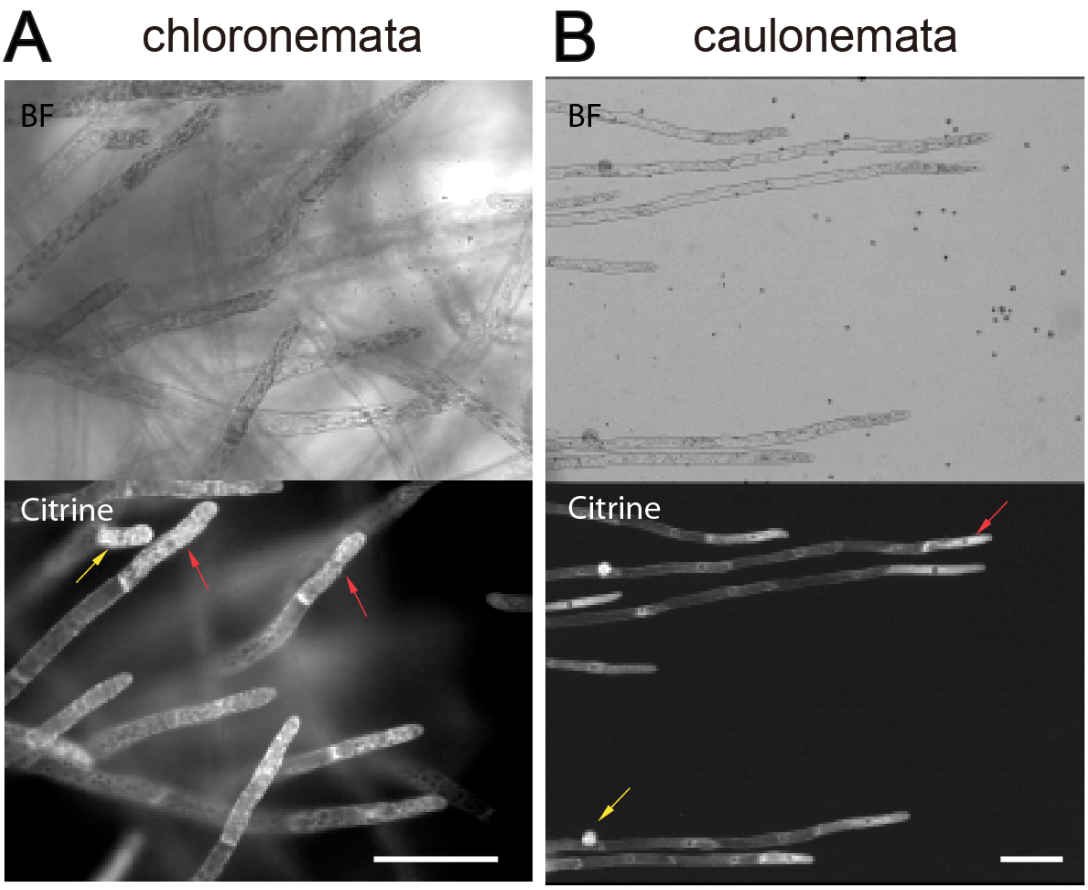

Figure 3. Predominant PpCSP1-Citrine signals in chloronema and caulonema apical stem cells

(A and B) Bright-field (BF) and fluorescence (Citrine) images of chloronemata (A) and caulonemata (B) of the nPpCSP1-Citrine-nosT #136 line. Red and yellow arrows indicate apical stem cells and side branch initial cells, respectively.
Scale bars represent 100 µm in (A) and (B).

(www.ncbi.nlm.nih.gov/Structure/cdd/wrpsb.cgi) identified a provisional domain PTZ00368 (universal minicircle sequence binding protein), which is comprised of two CCHC zinc-finger domains (Figure 4A). The presence of zinc-finger domains provides support to the hypothesis that PpCSP1 is a nucleic acid-binding protein. Most plant CSPs and some animal CSPs also have CCHC zinc-finger domains but bacteria CSPs do not. Then BLASTP searches using PpCSP1 sequence as a query were performed to identify proteins closely related to PpCSP1. Lin28 proteins, which have a CSD and two CCHC zinc-finger domains (Figure 4A), were the top hits when the BLAST searches were performed against the database of metazoan species, such as *Homo sapiens*, *Mus musculus*, and *Caenorhabditis elegans*. Subsequently, phylogenetic relationships of PpCSP1 and other proteins with above three domains were inferred using the maximum likelihood tree reconstruction method of RAxML [67]. Although the low resolution of the phylogenetic tree cannot indicate whether PpCSP1 is orthologous or paralogous to Lin28 (Figure 4B), PpCSP1 and Lin28 should be the closely related proteins because of the shared domains and these results led me to investigate whether PpCSP1 plays a role similar to Lin28 in reprogramming differentiated cells to stem cells.

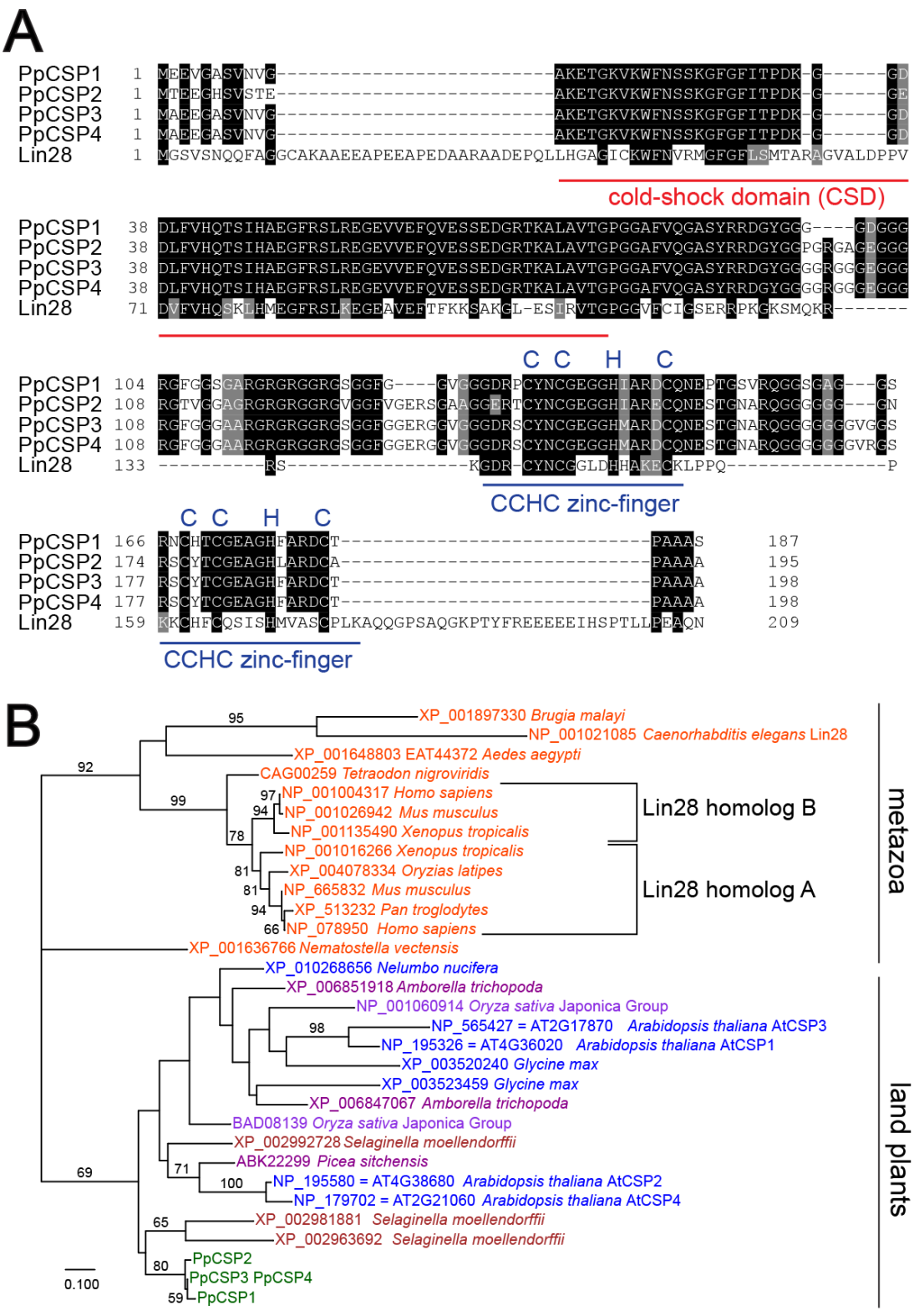
A
PpCSP1
PpCSP2
PpCSP3
PpCSP4
Lin28
cold-shock domain (CSD)
C C H C
CCHC zinc-finger
C C H C
CCHC zinc-finger
B
XP_001897330 Brugia malayi
NP_001021085 Caenorhabditis elegans Lin28
XP_001648803 EAT44372 Aedes aegypti
CAG00259 Tetraodon nigroviridis
NP_001004317 Homo sapiens
NP_001026942 Mus musculus
NP_001135490 Xenopus tropicalis
NP_001016266 Xenopus tropicalis
XP_004078334 Oryzias latipes
NP_665832 Mus musculus
XP_513232 Pan troglodytes
NP_078950 Homo sapiens
Lin28 homolog B
Lin28 homolog A
metazoa
XP_001636766 Nematostella vectensis
XP_010268656 Nelumbo nucifera
XP_006851918 Amborella trichopoda
NP_001060914 Oryza sativa Japonica Group
NP_565427 = AT2G17870 Arabidopsis thaliana AtCSP3
NP_195326 = AT4G36020 Arabidopsis thaliana AtCSP1
XP_003520240 Glycine max
XP_003523459 Glycine max
XP_006847067 Amborella trichopoda
BAD08139 Oryza sativa Japonica Group
XP_002992728 Selaginella moellendorffii
ABK22299 Picea sitchensis
NP_195580 = AT4G38680 Arabidopsis thaliana AtCSP2
NP_179702 = AT2G21060 Arabidopsis thaliana AtCSP4
XP_002981881 Selaginella moellendorffii
XP_002963692 Selaginella moellendorffii
land plants
PpCSP2
PpCSP3 PpCSP4
PpCSP1
0.100

Figure 4. PpCSP1 shares conserved domains with Lin28

(A) Alignment of the amino-acid sequences of PpCSPs and human Lin28 proteins. PpCSPs and human Lin28 proteins were predicted to contain one cold shock domain (CSD) (red line) and two CHCC zinc-finger domains (blue lines). Black and gray shades indicate identical amino acids and amino acids with similar characters to the consensus amino acid, respectively.
(B) Phylogeny of PpCSP1, Lin28, and related proteins with a cold-shock domain and zinc-finger domains. The maximum likelihood tree was constructed using amino-acid sequences of the proteins. The wag model of amino acid substitution was used. Branch lengths are proportional to the number of substituted residues. Bootstrap probability >50% is indicated on the branches (estimated by 1000 resampling). The accession numbers and species names are indicated. Color of the OTU represents the phylogenetic position: Orange, metazoans; Blue, eudicots; light purple, monocots; Dark purple, other seed plants including gymnosperms and basal angiosperms; Green, bryophytes; Brown, lycophytes. Mammalian *Lin28* genes used for the iPSC induction are included in Lin28 homolog A subfamily. Scale bar represents the amino-acid substitution rate per sites.

2.3.2 *PpCSP1* transcripts and protein accumulate during reprogramming

To investigate the function of *PpCSP1* in reprogramming, leaf cut assay was performed. In the leaf cut assay, leaves are cut from gametophores and cultivated on a medium without phytohormones [29]. Leaf cells facing the cut are reprogrammed to chloronema apical stem cells with tip growth and divide approximately 30 hours after excision [29] (Figure 1B). A chloronema apical stem cell divides to regenerate itself and form a chloronema subapical cell. Therefore, chloronema apical stem cells fulfill the definition of a stem cell: they self-renew and give rise to cells that go on to differentiate. All leaf cells with tip growth behave as chloronema apical stem cells [29] and the acquisition is the most reliable sign of the reprogramming at present. To examine the spatiotemporal expression pattern of the PpCSP1 protein in the cut leaves, the DNA fragment containing the nopaline synthase polyadenylation signal (nosT) and the neomycin phosphotransferase II (nptII) expression cassette was removed from the nPpCSP1-Citrine-nosT line by transiently expressing Cre recombinase [52]. As a result, the native 3’ UTR was fused to the *PpCSP1-Citrine* coding sequence (CDS) (nPpCSP1-Citrine-3’UTR line; Figure 2A). During the reprogramming process, Citrine signals specifically increased in leaf cells facing the cut just after excision (Figures 5A and 5B). The Citrine signals increased continuously until tip growth started. Even though the Citrine signals increased in most edge cells, fewer than half of the edge

cells protruded. These observations suggest that other factors unevenly distributed in the edge cells are also involved in reprogramming. After the protrusion, PpCSP1-Citrine signals localized more conspicuously at the phragmoplast than other parts in cytosol. The signals were dispersed in cytosol after cytokinesis with remaining signals at the cell septum. The signals at the phragmoplast decreased during subsequent cell divisions of chloronema apical stem cells (Figure 6). The signals were enriched after cell division in chloronema apical stem cells (Figure 5A). These indicate that PpCSP1 protein predominantly accumulates in the leaf cells facing the cut, accumulates during the reprogramming, gradually decreases after the reprogramming, and is maintained in stem cells. In addition, PpCSP1 was expressed in proliferating cells in gametophore apices where both stem cells and proliferating non-stem cells exist [28] (Figure 5D). This is reminiscent of Lin28 that regulates cell cycles in stem cells [68, 69]. PpCSP1-Citrine was localized in the cytosol but not in the nucleus (Figure 5C). Due to the presence of the CSD and zinc-finger domains, it is plausible that PpCSP1 functions as an RNA-binding protein to regulate mRNA maturation, stability, or translation in the cytosol in a manner similar to that reported for other CSPs [35, 36] , including Lin28 and related proteins in metazoa.

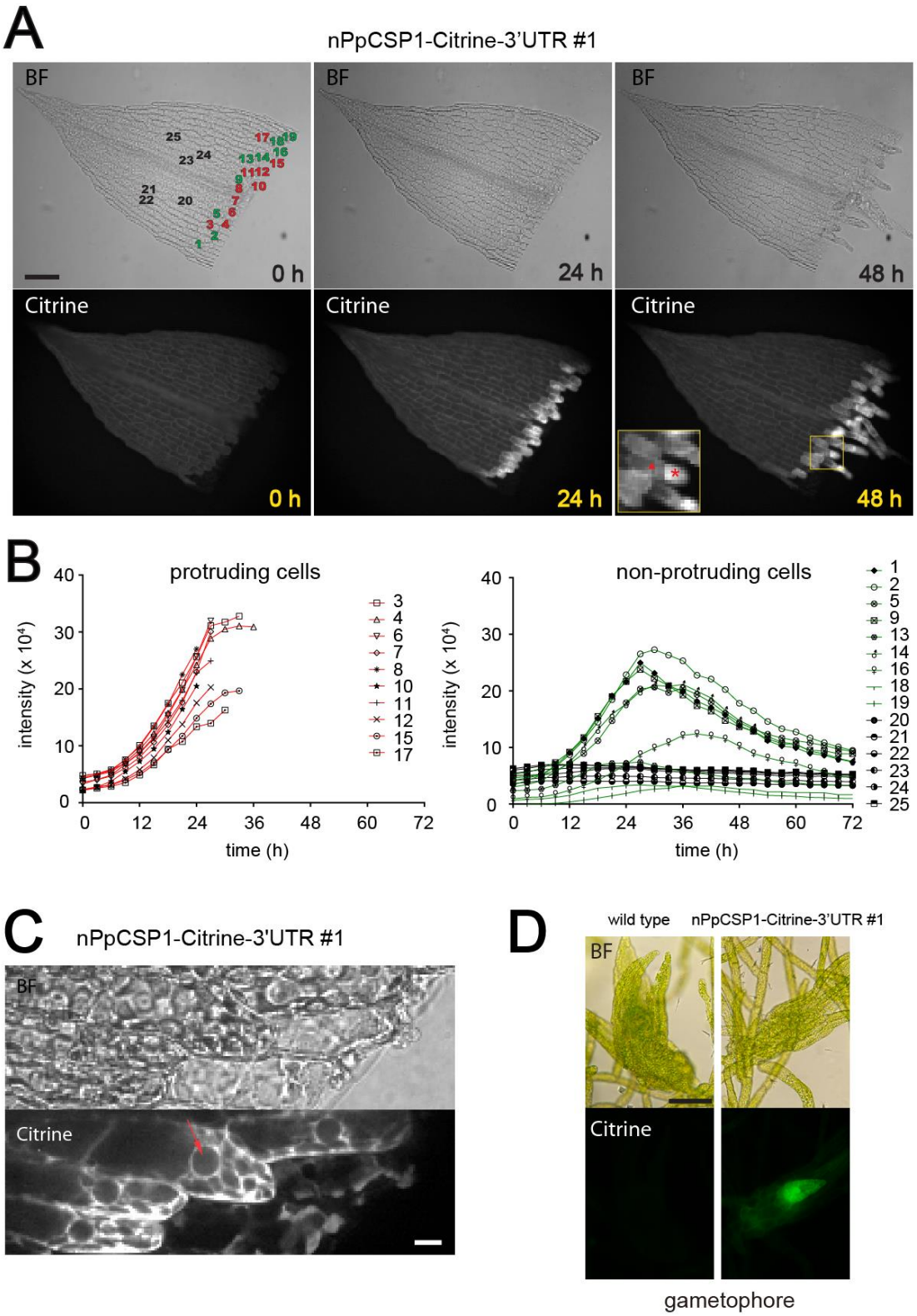
A
nPpCSP1-Citrine-3'UTR #1
BF
Citrine
0 h
24 h
48 h
B
protruding cells
non-protruding cells
intensity (x 10⁴)
time (h)
C
nPpCSP1-Citrine-3'UTR #1
D
wild type
nPpCSP1-Citrine-3'UTR #1
gametophore

Figure 5. PpCSP1 is induced in the process of reprogramming

(A) Expression pattern of PpCSP1-Citrine in an excised leaf of nPpCSP1-Citrine-3'UTR #1 line. Bright-field (BF) and fluorescent (Citrine) images at 0, 24, and 48 hours after cutting are shown. Inset red stars and triangles indicate a distal chloronema apical stem cell and a proximal chloronema cell, respectively. All edge cells and several non-edge cells were numbered for quantitative analysis in (B).
(B) The intensity of the Citrine signals in each cell of an excised leaf of nPpCSP1-Citrine-3'UTR #1 (1 to 25 correspond to cells in the top panel of [A]). Red and green lines indicate the signal intensity in edge cells that were and were not reprogrammed into stem cells, respectively. Black lines indicate the signal intensity in non-edge cells that were not reprogrammed into stem cells.
(C) PpCSP1-Citrine fusion protein localization in excised leaf cells 24 hours after cutting of the nPpCSP1-Citrine-3'UTR #1 line. Red arrow indicates the nucleus.
(D) Bright-field (BF) and fluorescent (Citrine) images of gametophore apices of the wild type and nPpCSP1-Citrine-3'UTR #1 line.
Scale bars represent 100 μm in (A), (D) and 10 μm in (C).

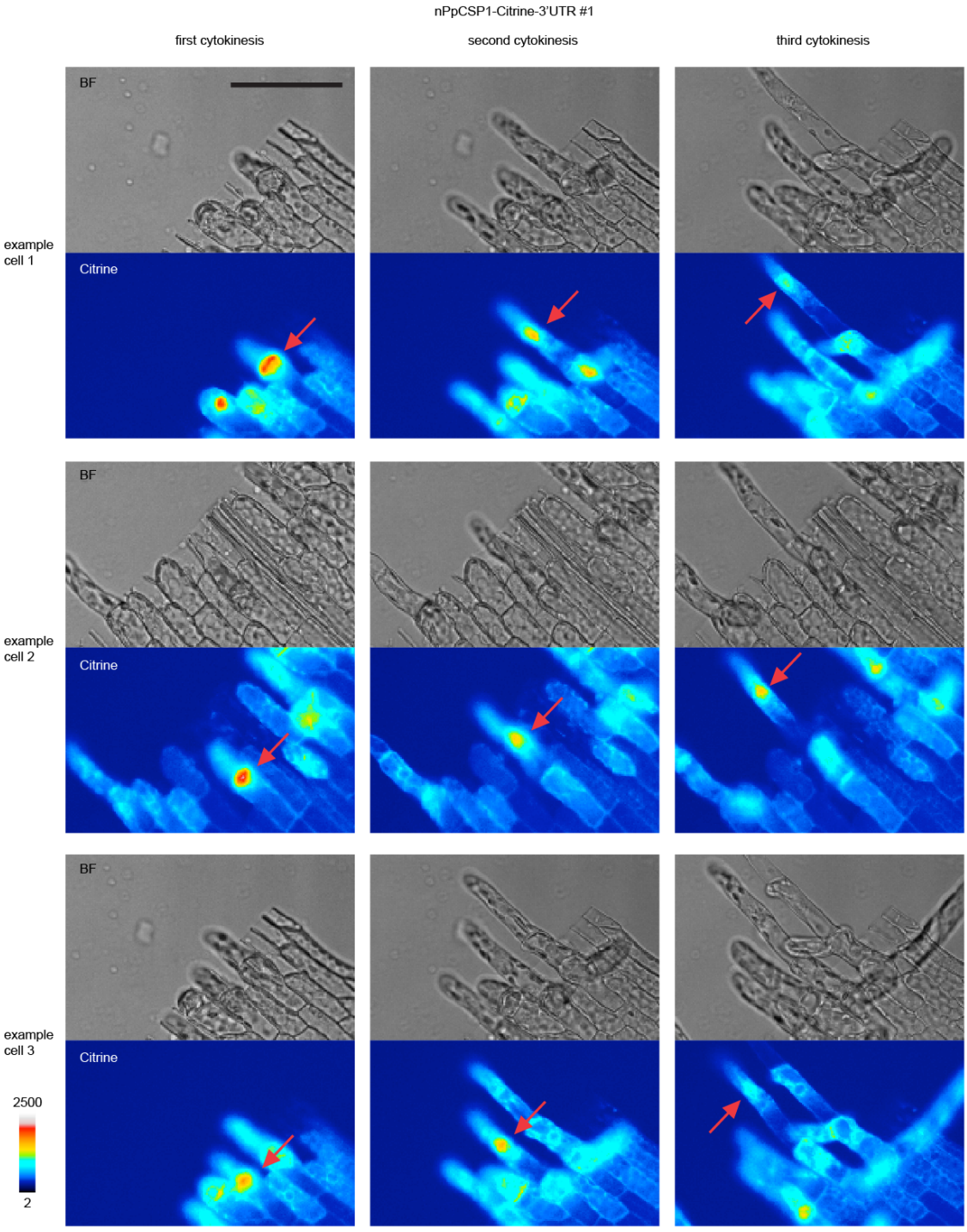
nPpCSP1-Citrine-3'UTR #1
first cytokinesis
second cytokinesis
third cytokinesis
example cell 1
example cell 2
example cell 3
BF
Citrine
2500
2

Figure 6. PpCSP1-Citrine protein localized at the phragmoplasts in excised leaf cells of nPpCSP1-Citrine-3'UTR #1 line

Initial three rounds of cytokinesis in chloronema apical stem cells reprogrammed from leaf cells are shown. Three chloronema apical stem cells from an excised leaf are shown. Red arrows indicate the phragmoplasts.
Scale bars represent 100 μm.

To analyze the promoter activity of *PpCSP1*, a transcriptional fusion (PpCSP1pro:LUC), in which the coding sequence of *luciferase* (*LUC*) [70] is driven by the 1.8-kb *PpCSP1* promoter was made. This construct was integrated into the PIG1 neutral site [53, 66] of the nPpCSP1-Citrine-3'UTR background line (Figures 2C and 2D). With this dual reporter construct (PpCSP1pro:LUC nPpCSP1-Citrine-3'UTR), simultaneous monitoring of the promoter activity and protein levels at a single-cell level was performed (Figures 7 and 8). Time-lapse imaging showed LUC signals from PpCSP1 promoter activity increasing after excision (Figure 7A). In edge cells that would later protrude, the intensities maximized at approximately 12 hours and were maintained with some fluctuation. However, the rates of increase and the maxima of the intensities varied among cells. In edge cells that never protruded, LUC signals initially increased but were not maintained as the protruded edge cells. PpCSP1-Citrine levels in cells that would protrude continued to increase from 24 to 36 hours, until these cells divided (Figure 7C). In edge cells that never protruded, Citrine accumulation reached a maximum in 24 to 36 hours and then gradually declined, which is consistent with the changes in promoter activity (Figure 7B). The smaller variation in protein levels than in promoter activity in cells that eventually protrude suggests the potential involvement of post-transcriptional regulation or the difference in stability of the transcripts and proteins of *PpCSP1*.

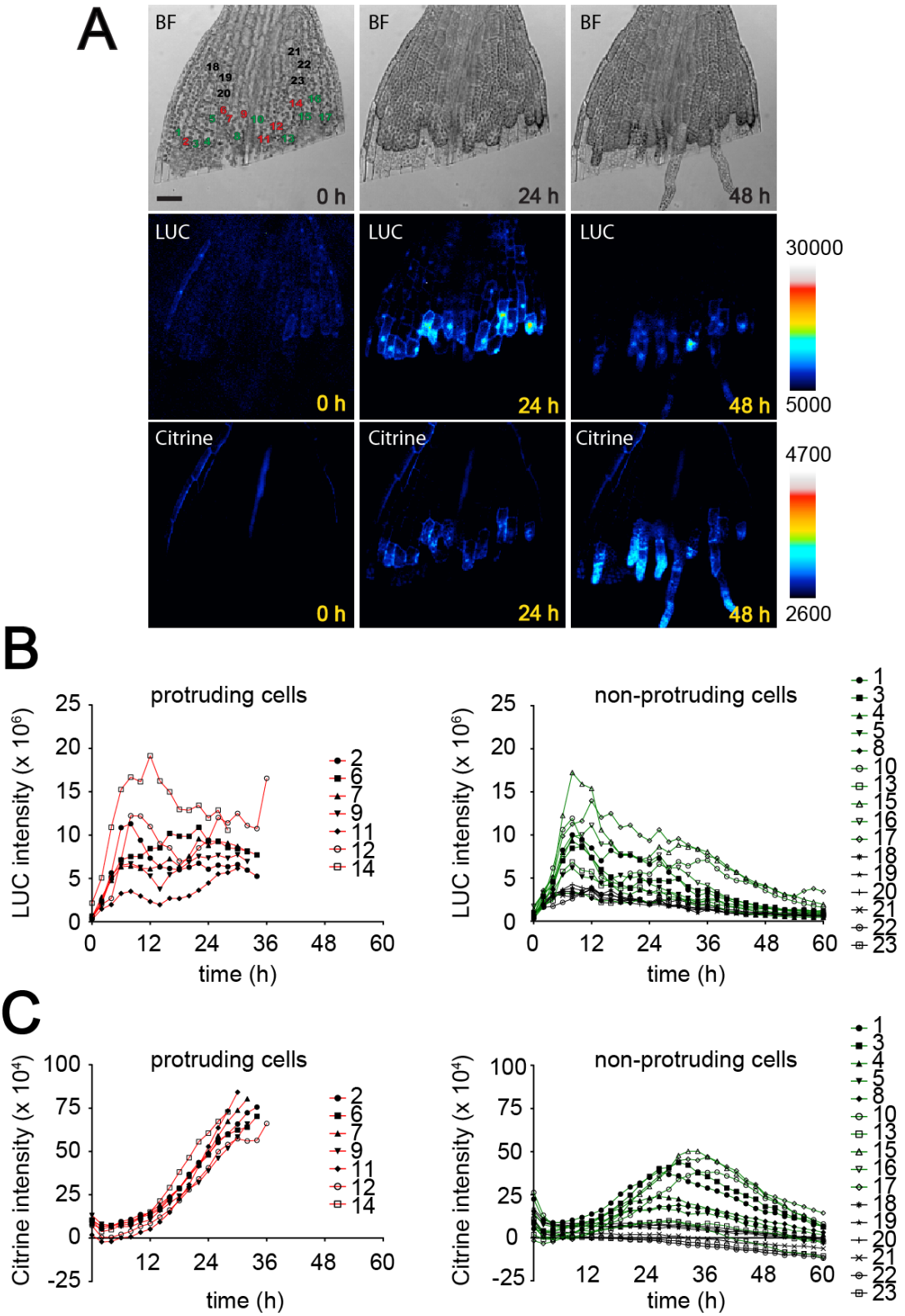
A
BF
0 h
24 h
48 h
LUC
30000
5000
Citrine
4700
2600
B
protruding cells
non-protruding cells
LUC intensity (x 10⁶)
time (h)
C
Citrine intensity (x 10⁴)

Figure 7. *PpCSP1* promoter activity and protein levels during the reprogramming

(A) *PpCSP1* promoter activity and the protein accumulation during the reprogramming. Bright-field (BF) (top), luciferase (middle) and Citrine images (bottom) of an excised leaf of the PpCSP1pro:LUC nPpCSP1-Citrine-3'UTR #2 line at 0, 24, and 48 hours after cutting. Calibration bars were shown for pseudo-color images of LUC and Citrine, respectively. All edge cells and several non-edge cells are numbered for (B) and (C).
(B and C) The intensity of luciferase (B) and Citrine (C) signals in each cell (indicated by 1 to 23 in the top left panel of [A]) in an excised leaf. Red and green lines indicate the signal intensity in edge cells that were and were not reprogrammed into stem cells, respectively. Black lines indicate the signal intensity in non-edge cells that were not reprogrammed into stem cells.
Scale bars represent 50 μm in (A).

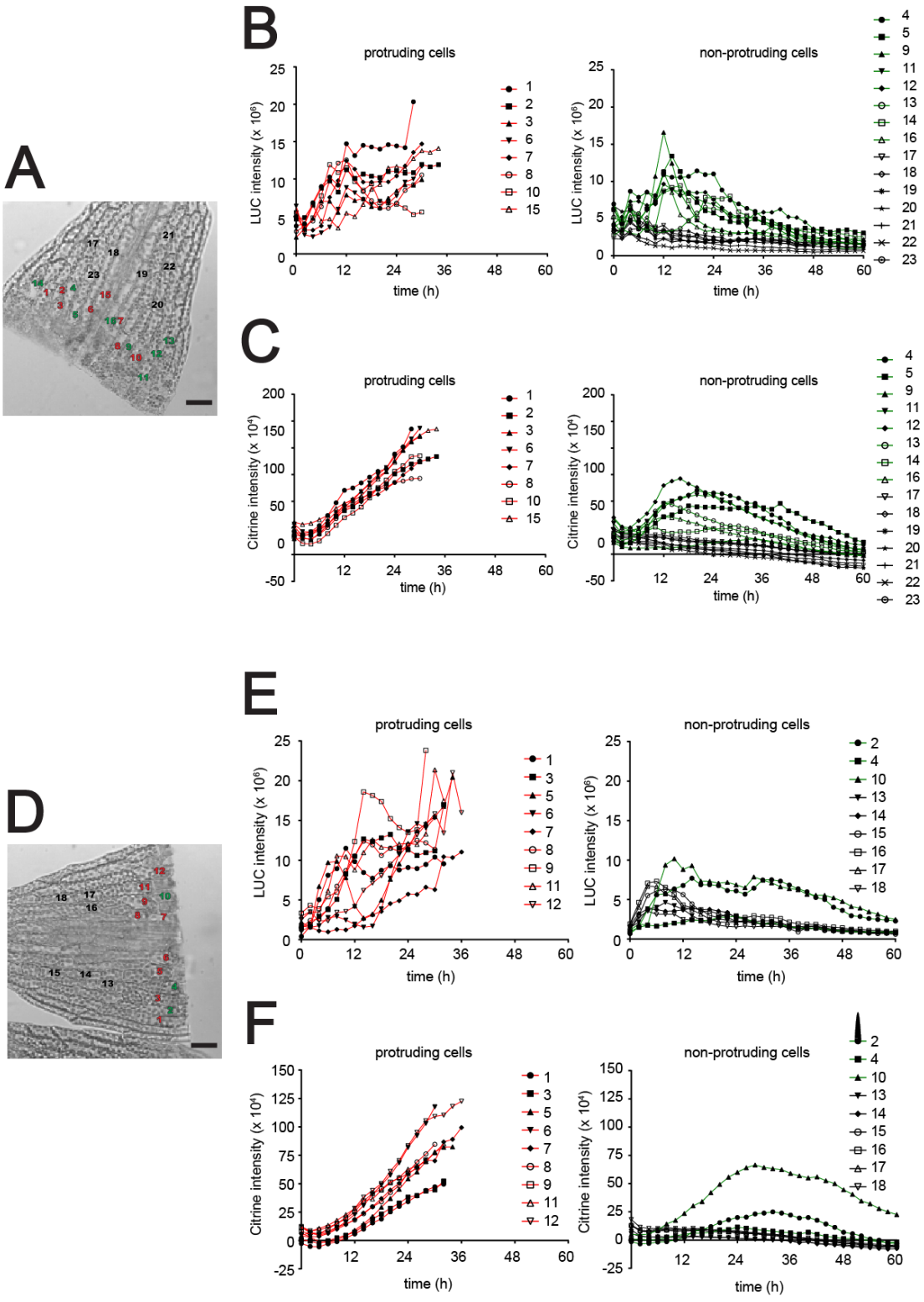
A
B
protruding cells
non-protruding cells
LUC intensity (x 10⁶)
time (h)
C
Citrine intensity (x 10⁴)
D
E
F

Figure 8. Replicates of quantitative analysis of *PpCSP1* promoter activity and the protein amount during the reprogramming

(A and D) Cut leaves of the PpCSP1pro:LUC nPpCSP1-Citrine-3'UTR #2 line used for the quantitative analysis of *PpCSP1* promoter activity and the protein amount during the reprogramming. All edge cells and several non-edge cells are numbered for (B and C) and (E and F), respectively.
(B-F) The intensity of luciferase (B and E) and Citrine (C and F) signals at each cell (indicated by 1 to 23 in [A] and 1 to 18 in [D], respectively) in excised leaves. Red and green lines indicate the signal intensity in edge cells that are and are not reprogrammed into stem cells, respectively. Black lines indicate the signal intensity in non-edge cells that are not reprogrammed into stem cells.
Scale bars represent 50 μm in (A) and (D).

2.3.3 *PpCSP1* is negatively regulated through its 3' UTR

Lin28 is negatively regulated by miRNA *let-7* [43-45, 71], which directly binds to *Lin28* transcripts at the 3' UTR leading to the degradation of the transcript [43]. In Physcomitrella genome, there is no miRNA similar to *let-7* [72-75]. However, the 3' UTR of *PpCSP1* is 623 bp, which is longer than the median length (334 bp) of 3' UTRs in the Physcomitrella v1.6 genome sequence [76]. This suggests that regulatory elements locate in the 3'UTR region. To determine if the 3' UTR of *PpCSP1* is involved in regulating transcript abundance, 5'-digital gene expression (5'-DGE) analysis was performed in the nPpCSP1-Citrine-3'UTR and nPpCSP1-Citrine-nosT lines, in which the 3' UTR is separated from the *PpCSP1* coding region by the nosT and the nptII resistance cassette (Figure 2A). These results were compared to previously published 5'-DGE data of leaf cut experiments [30] (Figure 9). In the 5'-DGE analysis, approximately 25 bp cDNA fragments at the 5'-ends of polyadenylated RNAs are sequenced. The tags in the 5' UTR or CDS represent RNA molecules that are not cut in the 3' UTR, while tags in the 3' UTR represent RNAs that are cut or undergoing degradation. The number of tags in the *PpCSP1* 5' UTR or CDS tended to increase after leaf cut and nPpCSP1-Citrine-nosT had a generally higher value than nPpCSP1-Citrine-3'UTR (6.6 fold in median, n=3). In wild-type and nPpCSP1-Citrine-3'UTR lines, more sequenced tags were mapped on the 3' UTR region than the 5' UTR or CDS, while in the

nPpCSP1-Citrine-nosT line more tags were mapped on the 5’ UTR or CDS than on the exogenous 3’ UTR of nosT (Figure 9). These data suggest that the 3’ UTR of *PpCSP1* is a degradation target or has a poor polyadenylation signal.

To examine the activity of the 3’ UTR, independent of its original genomic context, constructs with a constitutively active elongation factor 1 alpha (*EF1α*) promoter [54]-driven *sGFP* [77], fused to either the *PpCSP1* 3’ UTR or nosT were generated and introduced into the PTA1 neutral site [54] (Figure 10). sGFP intensity in the EF1αpro:sGFP-nosT line increased in all of the examined leaf cells during reprogramming after cutting (Figures 11A and 11B). The increase of activity was more conspicuous in edge cells than in non-edge cells (Figure 11B). On the other hand, in the 3’ UTR fused line, cellular signals of both edge and non-edge cells (Figures 11C and 11D) were approximately 10 times weaker than those in the nosT fused line (Figures 11B and 11D; Figure 12). To examine the degradation activity of the 3’ UTR under unwounded conditions, sGFP signals were compared in protonemata and gametophores between the two lines (Figures 11E and 11F). In gametophores and protonemata, signals of the 3’ UTR fused line were weaker than those in the nosT fused line as in the reprogramming process. Reverse transcriptase-quantitative PCR (RT-qPCR) determined that transcript levels of *sGFP* were 67.3 ± 1.5 fold (mean ± SD, n=3) and 57.2 ± 3.1 fold (mean ± SD, n=3) higher in the nosT than the 3’ UTR line in gametophores and

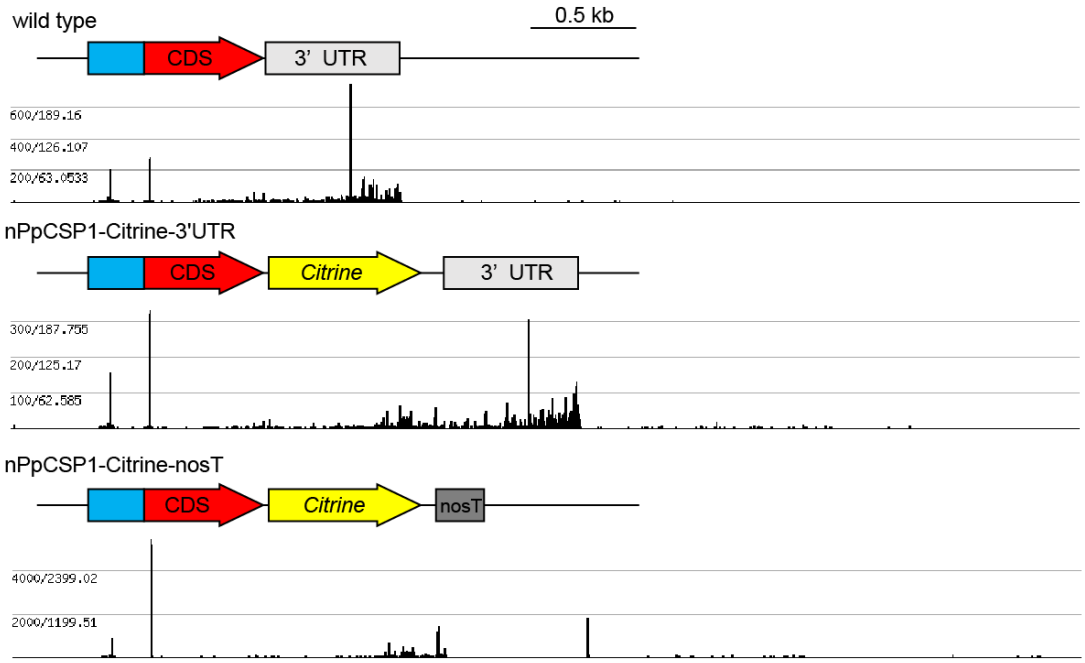

Figure 9. 5'-DGE transcriptome analysis of wild type, nPpCSP1-Citrine-3'UTR and nPpCSP1-Citrine-nosT lines

Location of 5' end of *PpCSP1* and *PpCSP1-Citrine* transcripts in wild type, nPpCSP1-Citrine-3'UTR and nPpCSP1-Citrine-nosT lines, respectively, detected by 5'-DGE transcriptome analysis. Sequence reads of full-length mRNAs were mapped around the transcription start site of the gene, and those of degraded mRNAs were mapped to other region of the transcript.

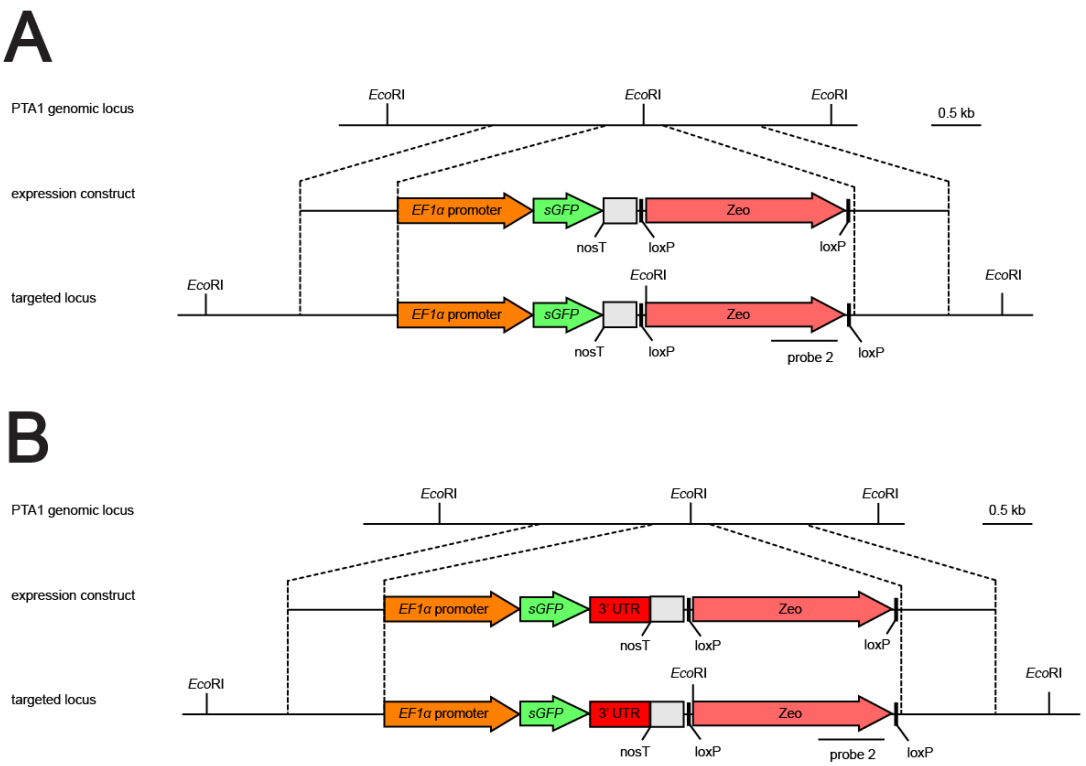
A
PTA1 genomic locus
EcoRI
EcoRI
EcoRI
0.5 kb
expression construct
EF1α promoter
sGFP
Zeo
nosT
loxP
loxP
targeted locus
EcoRI
EcoRI
EcoRI
EF1α promoter
sGFP
Zeo
nosT
loxP
probe 2
loxP
B
PTA1 genomic locus
EcoRI
EcoRI
EcoRI
0.5 kb
expression construct
EF1α promoter
sGFP
3' UTR
Zeo
nosT
loxP
loxP
targeted locus
EcoRI
EcoRI
EcoRI
EF1α promoter
sGFP
3' UTR
Zeo
nosT
loxP
probe 2
loxP
C
(kb)
wild type
EF1α:sGFP-nosT #3
EF1α:sGFP-nosT #4
EF1α:sGFP-3'UTR #18
EF1α:sGFP-3'UTR #19
10
8
6
4
2
probe 2

Figure 10. Construction of the EF1αpro:sGFP-nosT and EF1αpro:sGFP-3'UTR lines

(A and B) Schematic showing the insertion of a *sGFP* reporter gene driven by the *EF1α* promoter into the PTA1 locus with nosT (A) or 3' UTR of *PpCSP1* gene (B). Orange, green, and pink arrows indicate *EF1α* promoter [54], *sGFP* gene [77], and zeocin resistance cassette (Zeo) [78], respectively. Gray, black, and red boxes denote nosT, loxP, and *PpCSP1* 3' UTR, respectively. The probe used in (C) is indicated.
(C) DNA gel-blot analysis of targeted lines. Genomic DNA of wild type, EF1αpro:sGFP-nosT (#3 and #4), and EF1αpro:sGFP-3'UTR (#18 and #19) lines was digested with *Eco*RI.

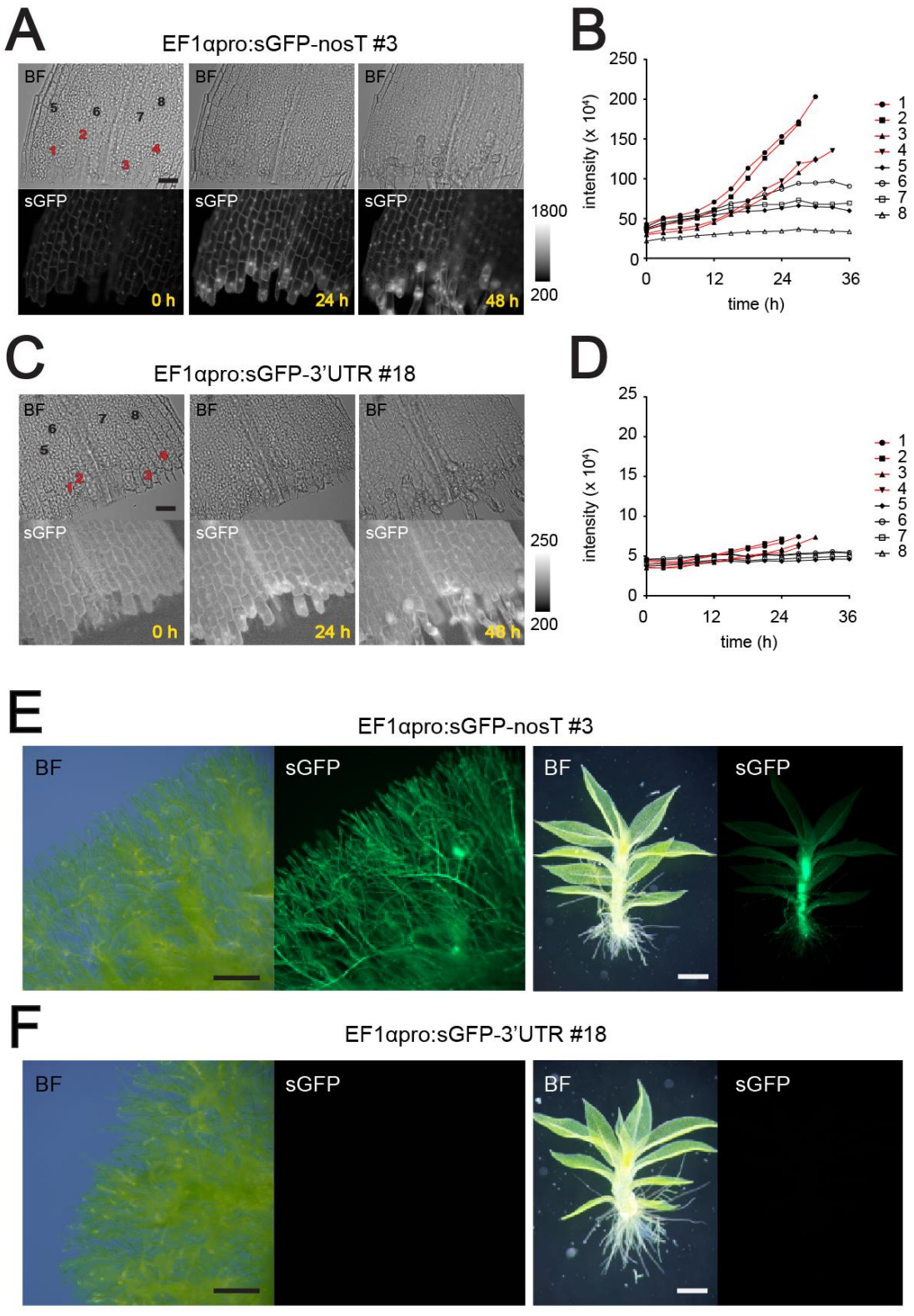
A
EF1αpro:sGFP-nosT #3
BF
sGFP
0 h
24 h
48 h
1800
200
B
intensity (x 10⁴)
time (h)
C
EF1αpro:sGFP-3'UTR #18
D
E
EF1αpro:sGFP-nosT #3
F
EF1αpro:sGFP-3'UTR #18

Figure 11. 3’ UTR of *PpCSP1* gene has a universal degradation function

(A and C) Bright-field (BF) and sGFP images of an excised leaf of EF1αpro:sGFP-nosT #3 (A) and EF1αpro:sGFP-3’UTR #18 (C) at 0, 24, and 48 hours after cutting. Several edge and non-edge cells are numbered for (B) and (D), respectively.
(B and D) The intensity of the sGFP signals in each cell of an excised leaf of EF1αpro:sGFP-nosT #3 (A) and EF1αpro:sGFP-3’UTR #18 (C) (numbers correspond to cells in the top panels of [A] and [C]), respectively. Red and black lines indicate the sGFP intensity in cells that were and were not reprogrammed into stem cells, respectively.
(E and F) Bright-field (BF) and fluorescent images of EF1αpro:sGFP-nosT #3 and EF1αpro:sGFP-3’UTR #18 in protonemata and a gametophore, respectively.
Scale bars represent 50 μm in (A) and (C), 500 μm in (E) and (F).

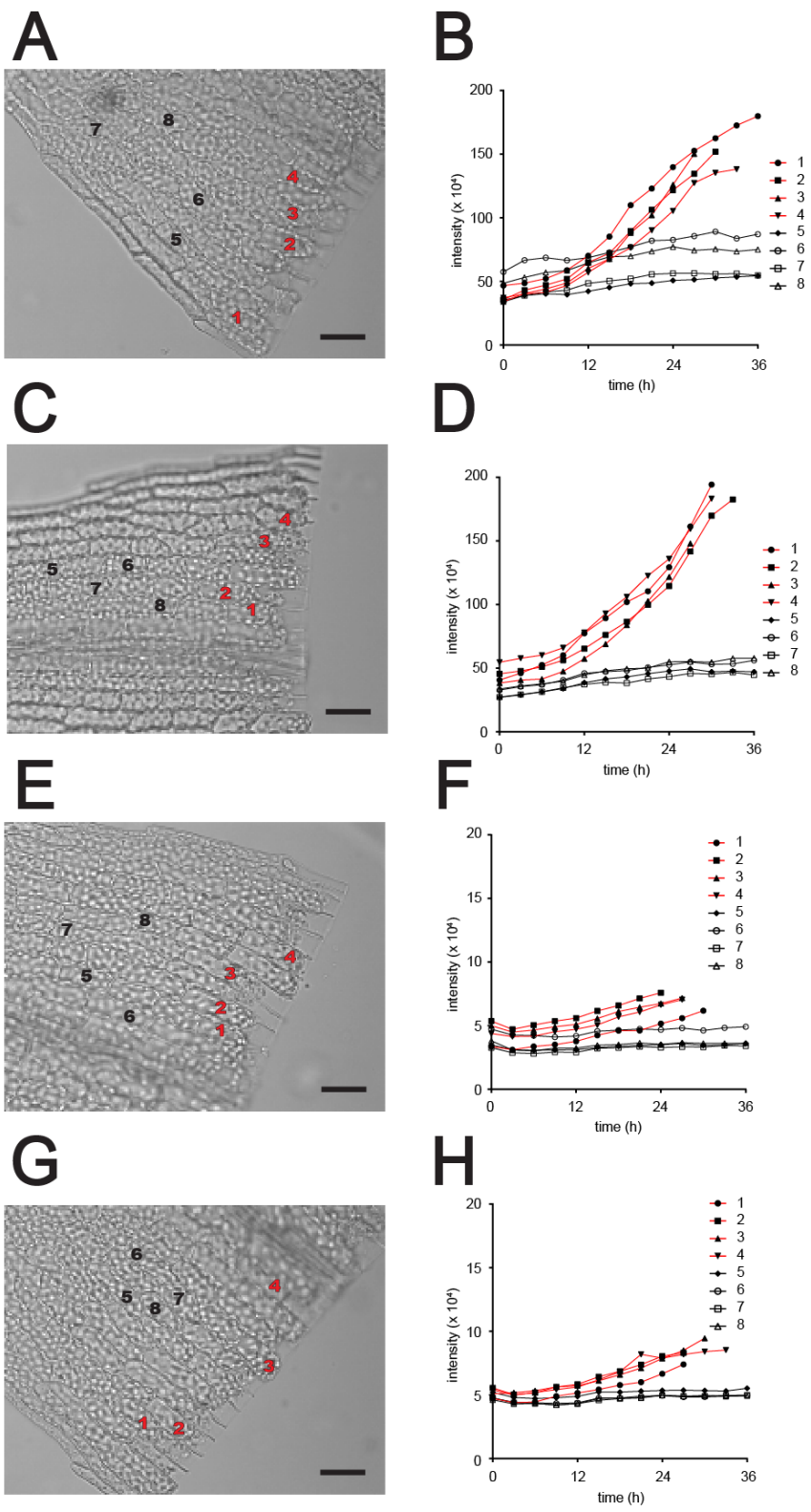
A
B
C
D
E
F
G
H
intensity (x 10⁴)
time (h)
0
12
24
36
50
100
150
200
5
10
15
20
1
2
3
4
5
6
7
8

Figure 12. Replicates of quantitative analysis of sGFP signals of EF1αpro:sGFP-nosT and EF1αpro:sGFP-3'UTR lines

(A, C, E, and G) Cut leaves of EF1αpro:sGFP-nosT #3 (A and C) and EF1αpro:sGFP-3'UTR #18 (E and G) lines for quantitative analysis of sGFP signals. Several edge and non-edge cells are numbered.
(B, D, F, and H) The intensity of the sGFP signals in each cell of an excised leaf of EF1αpro:sGFP-nosT #3 (B and D) and EF1αpro:sGFP-3'UTR #18 (F and H) (1 to 8 correspond to cells in [A], [C], [E] and [G], respectively). Red and black lines indicate the sGFP intensity in cells that are and are not reprogrammed into stem cells, respectively. Scale bars represent 50 μm in (A), (C), (E), and (G).

protonemata, respectively. These results indicate that the *PpCSP1* 3' UTR contains negative regulatory signals that function, independently of the *PpCSP1* promoter, during the reprogramming process in cut leaves, as well as during regular development.

2.3.4 *PpCSP1* does not appear to be regulated by a microRNA

miRNAs evolved independently in land plants and metazoa [79-81]. However, some similarities exist between these two linages, such as conserved components like Dicer/Dicer-like and Argonaute proteins [79]. In addition, two possible Arabidopsis miRNAs (miRNA854 and miRNA855) were identified to be shared between land plants and metazoa and had binding sites within the 3' UTR of the target mRNA [82]. To test whether a similar miRNA-associated regulation to *let-7* miRNA to the *PpCSP1* 3' UTR, a deletion series of the 3' UTR fusing each fragment after the stop codon of a *sGFP* reporter gene driven by the constitutive rice *Actin 1* promoter was made [83, 84] (Figure 13A). These constructs were transiently introduced into gametophore leaf cells by particle bombardment and co-bombarded with a fragment containing the *monomeric Red Fluorescent Protein 1* (*mRFP*) gene [85] driven by the same *Actin 1* promoter for normalization (Figures 13A and 13B). The linearity of the sGFP and mRFP signals in the transformed cells was confirmed (Figure 13C). In comparison to the control (no UTR), signal intensities of sGFP fused with

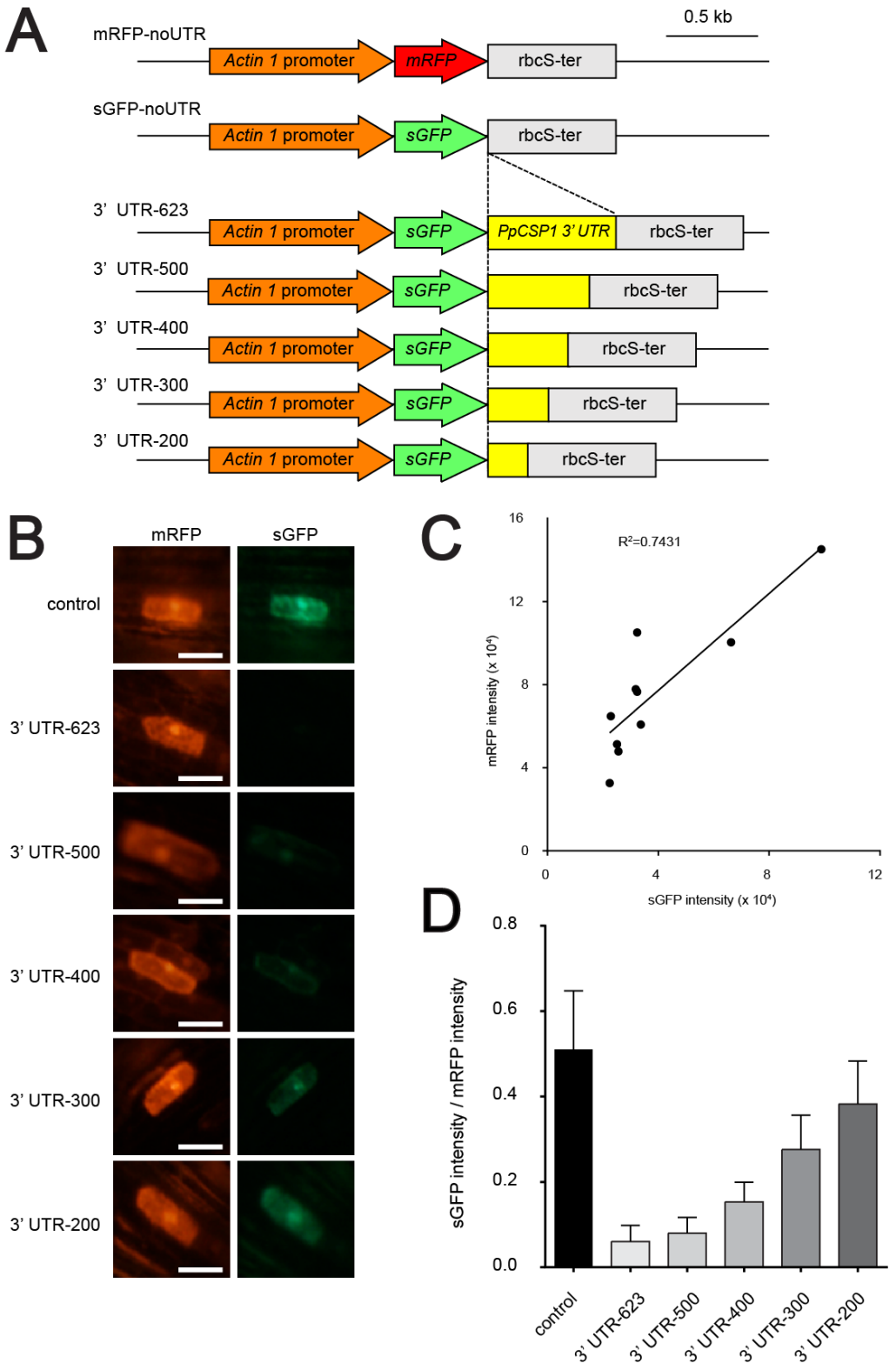
A
0.5 kb
mRFP-noUTR
Actin 1 promoter
mRFP
rbcS-ter
sGFP-noUTR
sGFP
3' UTR-623
PpCSP1 3' UTR
3' UTR-500
3' UTR-400
3' UTR-300
3' UTR-200
B
mRFP
sGFP
control
C
R²=0.7431
mRFP intensity (x 10⁴)
sGFP intensity (x 10⁴)
D
sGFP intensity / mRFP intensity

Figure 13. Function analysis of series deletion of the *PpCSP1* 3' UTR

(A) Schematics of the introduced fragments. Series of the *PpCSP1* 3' UTR with different lengths (yellow boxes) were connected to *sGFP* (green arrows), which is constitutively expressed by the rice *Actin 1* promoter (orange arrows). These deletion constructs were introduced into Physcomitrella leaf cells with mRFP (red arrow) fragments (shown at the top) by particle bombardment.
(B) Representative cells with mRFP (red) and sGFP (green) signals with constructs shown in (A).
(C) Linear correlation of the sGFP and mRFP [85] signals in the cells transformed with both constructs. X- and Y-axes indicate the fluorescence intensity of sGFP and mRFP, respectively.
(D) Ratio of sGFP intensity to co-transformed mRFP intensity in each transformed cell (n = 10). Error bars represent SD.
Scale bars represent 50 μm in (B).

623-, 500-, 400-, 300-, and 200-bp 3’ UTR fragments decreased to 11.8%, 15.7%, 29.4%, 54.9%, and 74.5%, respectively (Figure 13D). This gradual reduction suggests that several different regions in the 3’ UTR serve as targets for the negative regulation. Candidate miRNAs were subsequently searched using the 3’ UTR as a query in the psRNATarget website (http://plantgrn.noble.org/psRNATarget/) [86] and analyzed small RNAs at *PpCSP1* locus in Plant Small RNA Genes WebServer (https://plantsmallrnagenes.psu.edu/cgi-bin/Ppatens_Locus_Reporter) [72]. However, no miRNA targeting sequences in the 3’ UTR was found. In the future, additional studies such as genome-wide mRNA-protein interaction analysis [87], will be needed to fully understand the molecular mechanisms of the degradation function of the *PpCSP1* 3’ UTR.

2.3.5 Increase of *PpCSP1* transcript level enhances reprogramming of non-edge cells

Having determined that the 3’ UTR has a degradation function, transcript levels in the nPpCSP1-Citrine-nosT line were quantified, and compared them to the nPpCSP1-Citrine-3’UTR line and wild type. Using RT-qPCR, transcript levels were 6.0 ± 2.9 fold (mean ± SD, n=3) and 9.9 ± 2.5 fold (mean ± SD, n=3) higher in the nPpCSP1-Citrine-nosT line as compared to the nPpCSP1-Citrine-3’UTR line and wild type at 0 h after leaf cutting, respectively. These results are in agreement with the 5’-DGE

analysis as the tag counts in nPpCSP1-Citrine-3'UTR were not drastically different when compared with wild type. Collectively, these results indicate that transcript levels of *PpCSP1* increased in the nPpCSP1-Citrine-nosT line.

As the *PpCSP1* transcript level is approximately 10-fold higher in the nPpCSP1-Citrine-nosT line, protruding non-edge cells were observed (Figure 14), while only edge cells protrude in wild type (Figure 1B). The percentages of excised leaves with at least one protruding non-edge cell in wild-type, nPpCSP1-Citrine-nosT, and nPpCSP1-Citrine-3'UTR lines were calculated (Figures 14A and 14B). While the percentages of excised leaves with protruding edge cells did not differ among these lines (Figure 14A), those with protruding non-edge cells significantly increased in nPpCSP1-Citrine-nosT (Figure 14B). Moreover, some non-edge cells of nPpCSP1-Citrine-nosT exhibited stronger Citrine signals than surrounding cells, some of which were reprogrammed to stem cells (Figures 14C and 14D; Figure 15), while Citrine signals of nPpCSP1-Citrine-3'UTR lines were detected in cells at the cut edge but not in non-edge cells (Figure 5A).

To confirm the increase in protruding non-edge cells in the nPpCSP1-Citrine-nosT line, a PpCSP1pro:PpCSP1-Citrine line was generated. In this construct, the *PpCSP1* promoter, *PpCSP1* CDS, and Citrine gene were inserted into the neutral PTA1 site

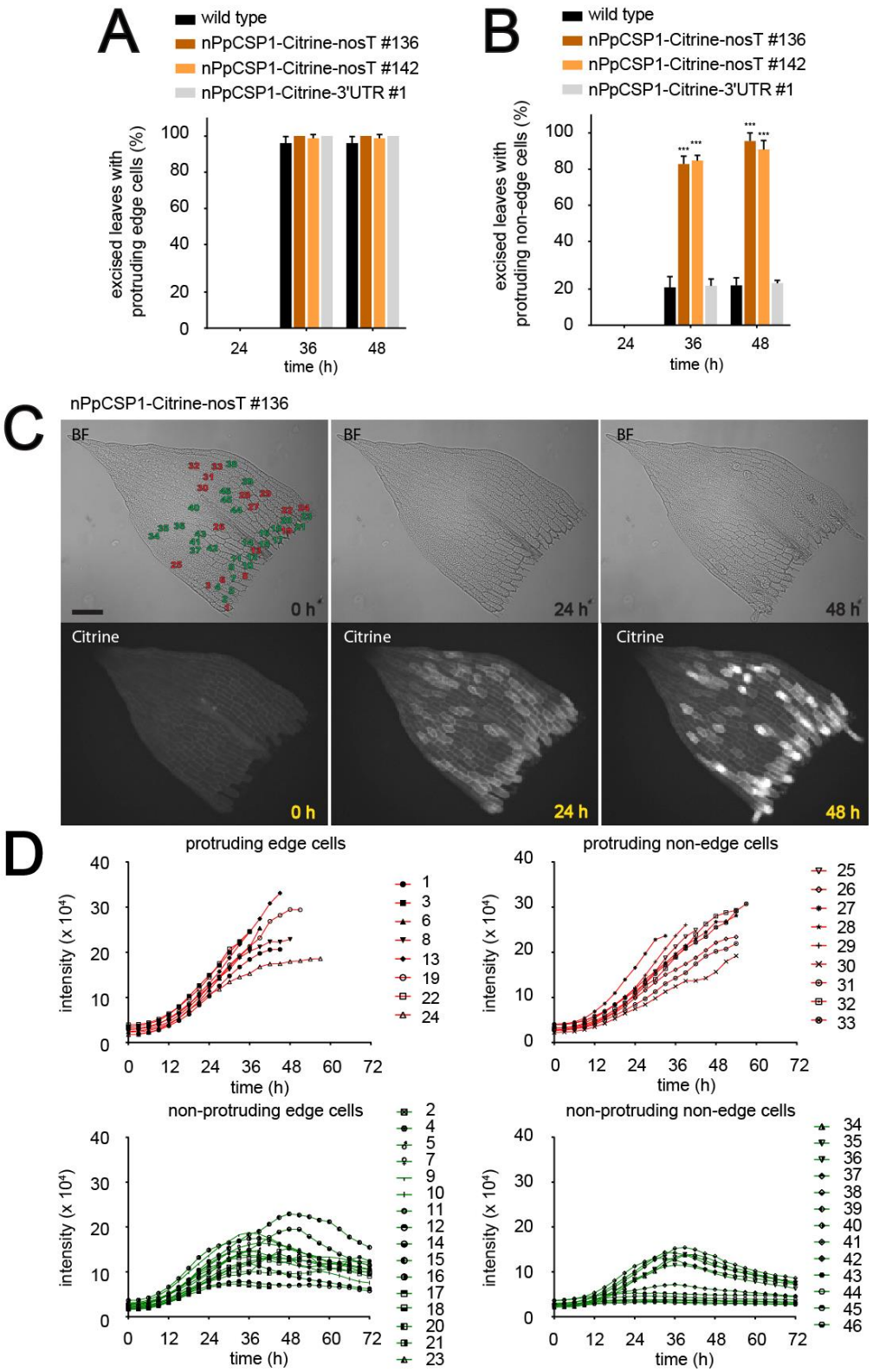
A
wild type
nPpCSP1-Citrine-nosT #136
nPpCSP1-Citrine-nosT #142
nPpCSP1-Citrine-3'UTR #1
excised leaves with protruding edge cells (%)
time (h)
B
excised leaves with protruding non-edge cells (%)
C
nPpCSP1-Citrine-nosT #136
BF
Citrine
0 h
24 h
48 h
D
protruding edge cells
protruding non-edge cells
non-protruding edge cells
non-protruding non-edge cells
intensity (x 10⁴)
time (h)

Figure 14. Increased PpCSP1 protein accumulation causes enhanced reprogramming

(A and B) Percentages of excised leaves with protruding edge cells (A) and protruding non-edge cells (B). Twenty leaves excised from wild type, nPpCSP1-Citrine-nosT (#136 and #142), and nPpCSP1-Citrine-3'UTR #1 were used for each analysis. Error bars represent SD from biological triplicates. ***$p < 0.001$ by Welch's *t*-test.
(C) Expression pattern of PpCSP1-Citrine in an excised leaf of nPpCSP1-Citrine-nosT #136. Bright-field and Citrine images at 0, 24, and 48 hours after cutting are shown. All edge cells and several non-edge cells are numbered for (D).
(D) The intensity of Citrine signals in each cell (numbers correspond to cells in the top panel of [C]) of an excised leaf of nPpCSP1-Citrine-nosT #136. Red and green lines indicate the intensities of Citrine signals in protruding and non-protruding cells, respectively.
Scale bars represent 100 μm in (C).

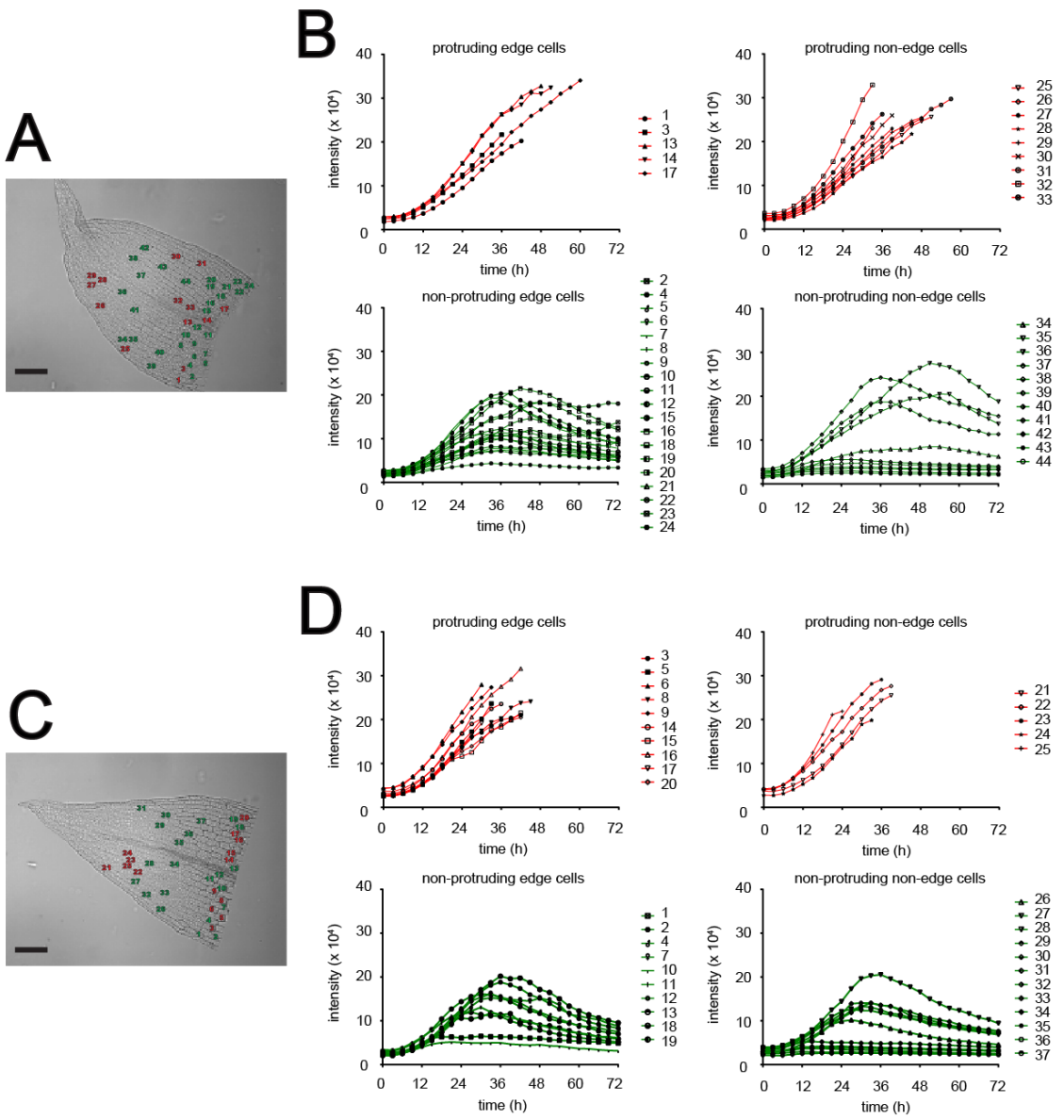

Figure 15. Replicates of quantitative analysis of Citrine signals of nPpCSP1-Citrine-nosT #136 line

(A and C) Cut leaves of nPpCSP1-Citrine-nosT #136 line used for the quantitative analysis. All edge cells and several non-edge cells are numbered for (B) and (D).

(B and D) The intensity of the Citrine signals in each cell (1 to 44 correspond to cells in [A]; 1 to 37 correspond to cells in [C], respectively) of excised leaves of nPpCSP1-Citrine-nosT #136. Red and green lines indicate intensities of Citrine signals in protruding and non-protruding cells, respectively.

Scale bars represent 100 μm in (A) and (C).

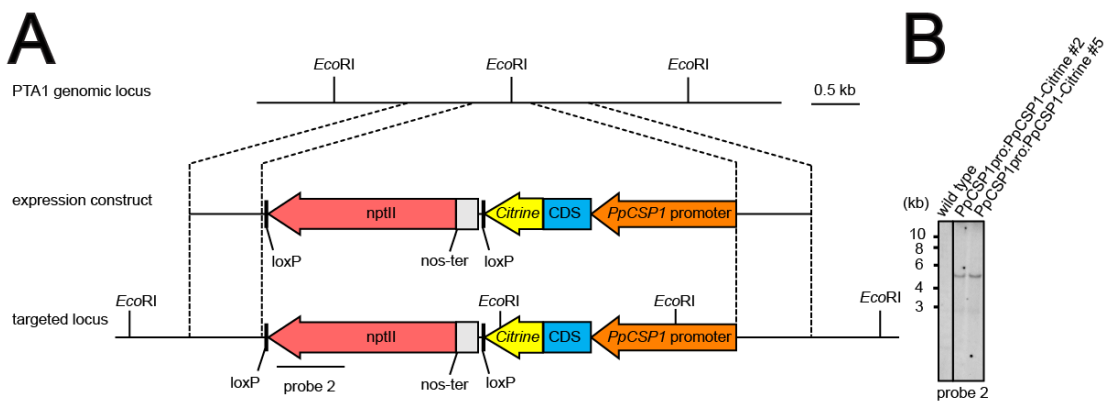

Figure 16. Construction of the PpCSP1pro:PpCSP1-Citrine lines

(A) Schematic showing the insertion of *PpCSP1* promoter-driven *PpCSP1-Citrine* fusion gene construct into the PTA1 locus. Orange, blue, yellow, and pink arrows denote the *PpCSP1* promoter, the *PpCSP1* coding sequence (CDS), *Citrine* CDS, and the nptII expression cassette, respectively. Gray and black boxes denote the nosT and the loxP sequence, respectively. The probe used in (B) is indicated.
(B) DNA gel-blot analysis of targeted lines. Genomic DNA of wild type and PpCSP1pro:PpCSP1-Citrine (#2 and #5) lines was digested with *Eco*RI.

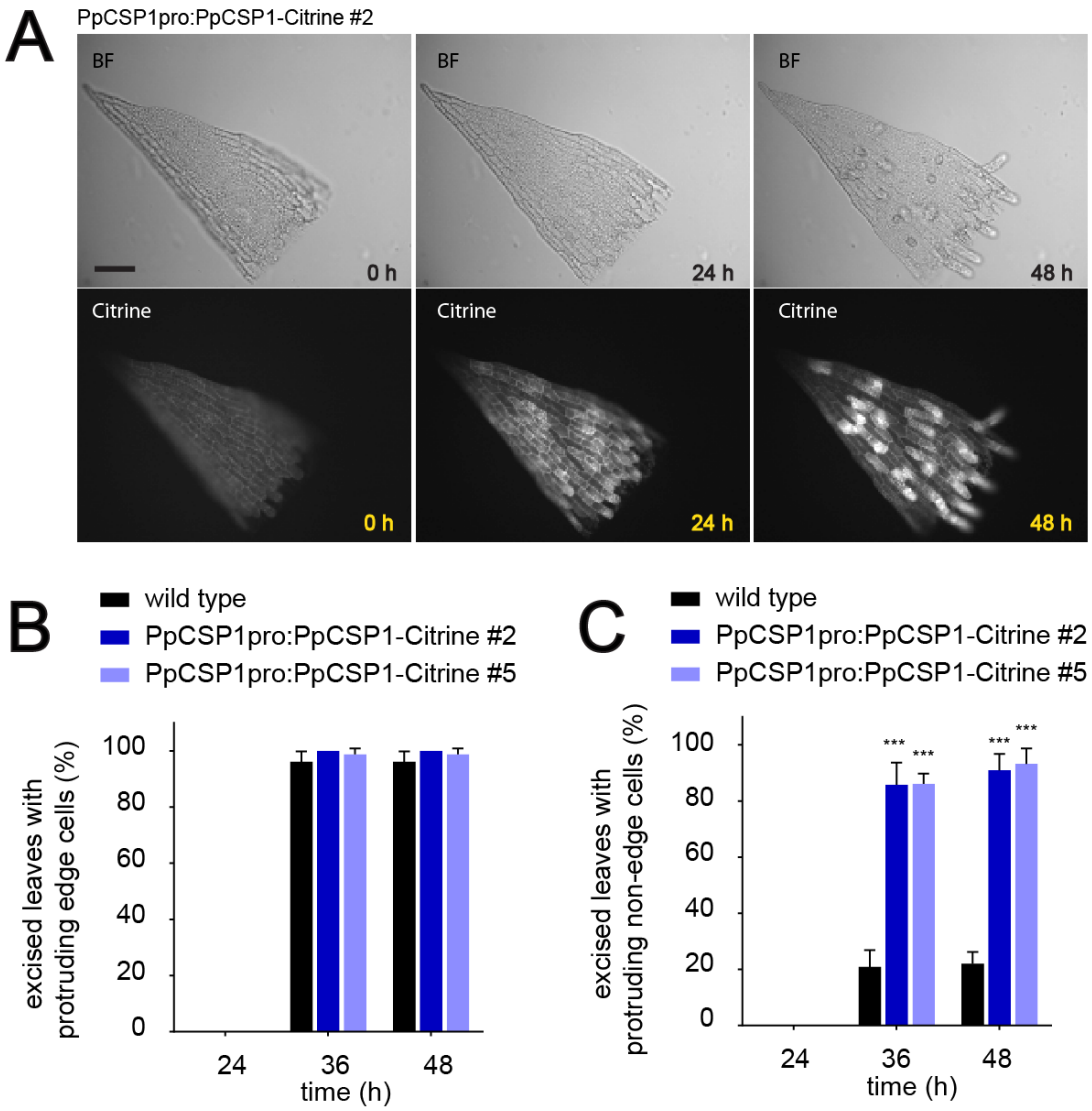

Figure 17. Phenotype analysis of PpCSP1pro:PpCSP1-Citrine line

(A) Expression patterns of PpCSP1-Citrine in an excised leaf of PpCSP1pro:PpCSP1-Citrine #2. Bright field (BF) and Citrine images at 0, 24, and 48 hours after cutting are shown.

(B and C) Percentage of excised leaves with protruding edge cells (B) and protruding non-edge cells (C). Twenty leaves were excised from wild type and PpCSP1pro:PpCSP1-Citrine (#2 and #5). Error bars represent the SD from biological triplicates. ***p < 0.001 by Welch's *t*-test.

Scale bars represent 100 µm in (A).

(Figure 16), which could be used to visualize increased PpCSP1-Citrine levels. RT-qPCR analysis indicated that transcript levels of *PpCSP1* were 15.5 ± 3.7 fold (mean ± SD, n=3) higher in PpCSP1pro:PpCSP1-Citrine as compared to wild type at 0 h after leaf cutting. Spatiotemporal patterns of Citrine signals and protruding cells in the PpCSP1pro:PpCSP1-Citrine line were similar to those of the nPpCSP1-Citrine-nosT line (Figure 17). These conclude that the protruding non-edge cell phenotype resulted from increased transcript levels of *PpCSP1-Citrine*. On the other hand, there were no morphological and growth differences in protonemata and gametophores between wild-type and nPpCSP1-Citrine-nosT lines (Figure 21).

To investigate the relationship between *PpCSP1* and other factors involved in the reprogramming, transcript levels of *WOX13-like* genes [31] in nPpCSP1-Citirine-3'UTR and nPpCSP1-Citrine-nosT lines were analyzed with 5'-DGE during the reprogramming of cut leaves. However, no significant differences were observed in the transcript levels (Figure 18A and 18B). On the other hand, *PpCSP1* transcript levels investigated with the 5'-DGE data in Δ*ppwox13lab* line [31] were detected to be lower than those in wild type at 24 hours after dissection, while *PpCSP1* transcripts were similarly induced until 6 hours in wild type and the mutant (Figure 18C). These results suggest that *PpCSP1* is positively regulated by *WOX13-like* genes but *PpCSP1* does not regulate *WOX13-like* genes.

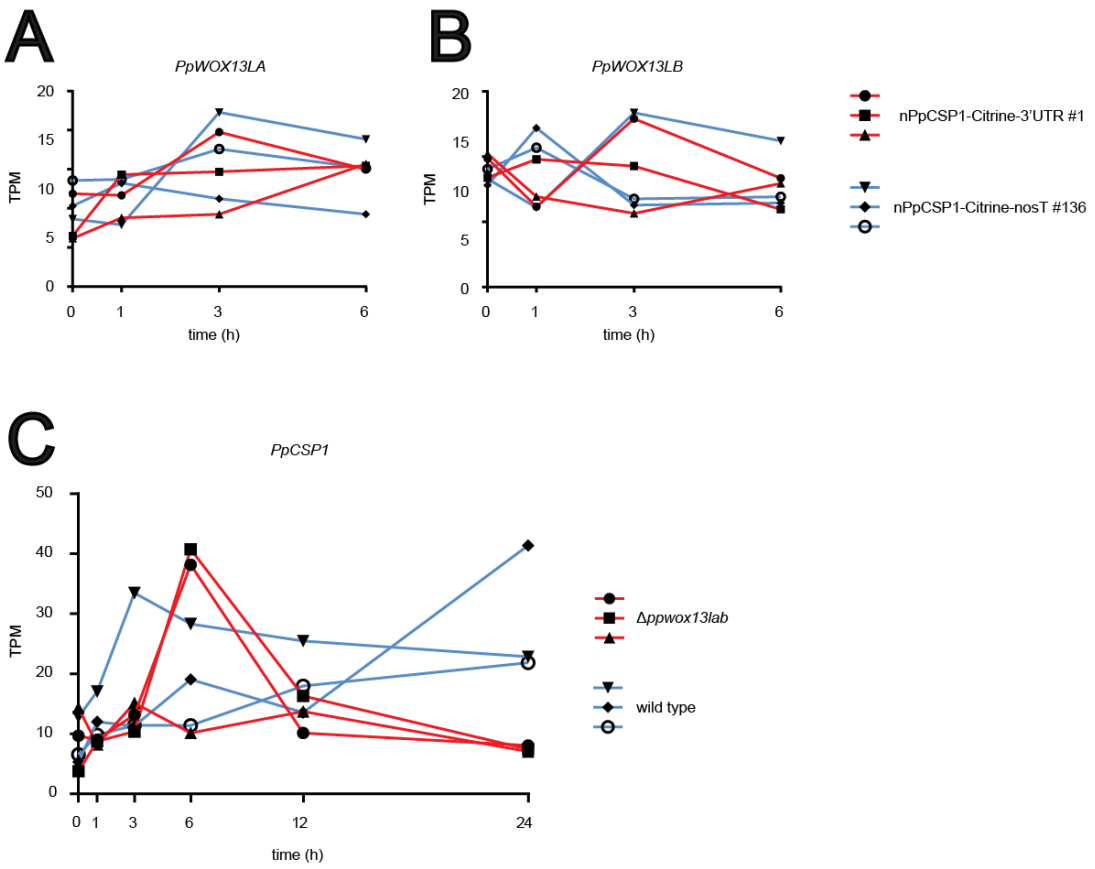
A
PpWOX13LA
TPM
time (h)
B
PpWOX13LB
TPM
time (h)
nPpCSP1-Citrine-3'UTR #1
nPpCSP1-Citrine-nosT #136
C
PpCSP1
TPM
time (h)
Δppwox13lab
wild type

Figure 18. Transcript levels of *PpWOX13L* genes in nPpCSP1-Citrine-3'UTR and nPpCSP1-Citrine-nosT lines and those of *PpCSP1* gene in the wild type and Δ*ppwox13lab* lines

(A and B) Transcript levels of *PpWOX13LA* and *PpWOX13LB* genes in nPpCSP1-Citrine-3'UTR and nPpCSP1-Citrine-nosT lines. Horizontal axes indicate the time after leaf excision and vertical axes indicate tags per million (TPM) values in 5'-DGE analysis. Red and blue lines indicate transcript levels in the nPpCSP1-Citrine-3'UTR and nPpCSP1-Citrine-nosT lines, respectively. Results of three independent experiments are shown.
(C) Transcript levels of *PpCSP1* gene in wild type and Δ*ppwox13lab* line. Horizontal axis indicates the time after leaf excision and vertical axis indicates tags per million (TPM) values in 5'-DGE analysis [31]. Blue and red lines indicate transcripts levels in the wild type and Δ*ppwox13lab* line, respectively. Results of three independent experiments are shown.

2.3.6 A *PpCSP* quadruple deletion mutant exhibits attenuated reprogramming

Deletion of the *PpCSP1* gene (Figure 19A) resulted in no detectable difference in reprogramming (Figures 20A and 20B). There are three closely related genes, *PpCSP2*, *PpCSP3*, and *PpCSP4*, (Figure 4A) in the Physcomitrella genome [25, 88]. Single (*ppcsp2*, *ppcsp3*, and *ppcsp4*), double (*ppcsp1 ppcsp2*), triple (*ppcsp1 ppcsp2 ppcsp3*), and quadruple (*ppcsp1 ppcsp2 ppcsp3 ppcsp4*) deletion mutants were generated (Figures 19). The percentage of excised leaves with reprogrammed cells was similar to wild type in all single, double, and triple deletion mutant lines in both edge and non-edge cells (Figures 20A and 20B). However, in the quadruple deletion mutant lines, cell protrusion was delayed (Figure 20C). The delay was more severe in non-edge cells and was significant until 72 hours (Figures 20C and 20D), when chloronemata covered the excised leaves and further observation was impossible. Collectively, these results indicate that the four PpCSP genes are positive regulators of stem cell formation and possess redundant functions.

PpCSP1 was expressed in not only stem cells but also proliferating non-stem cells in gametophore apices (Figure 5D) and appeared to localize at the phragmoplast (Figure 6). These data suggest the possibility that PpCSP1 is not involved in the reprogramming but in general cell cycle progression. To examine this possibility, the phenotype of the quadruple deletion mutant and the *PpCSP1* transcript-increased line in protonemata and

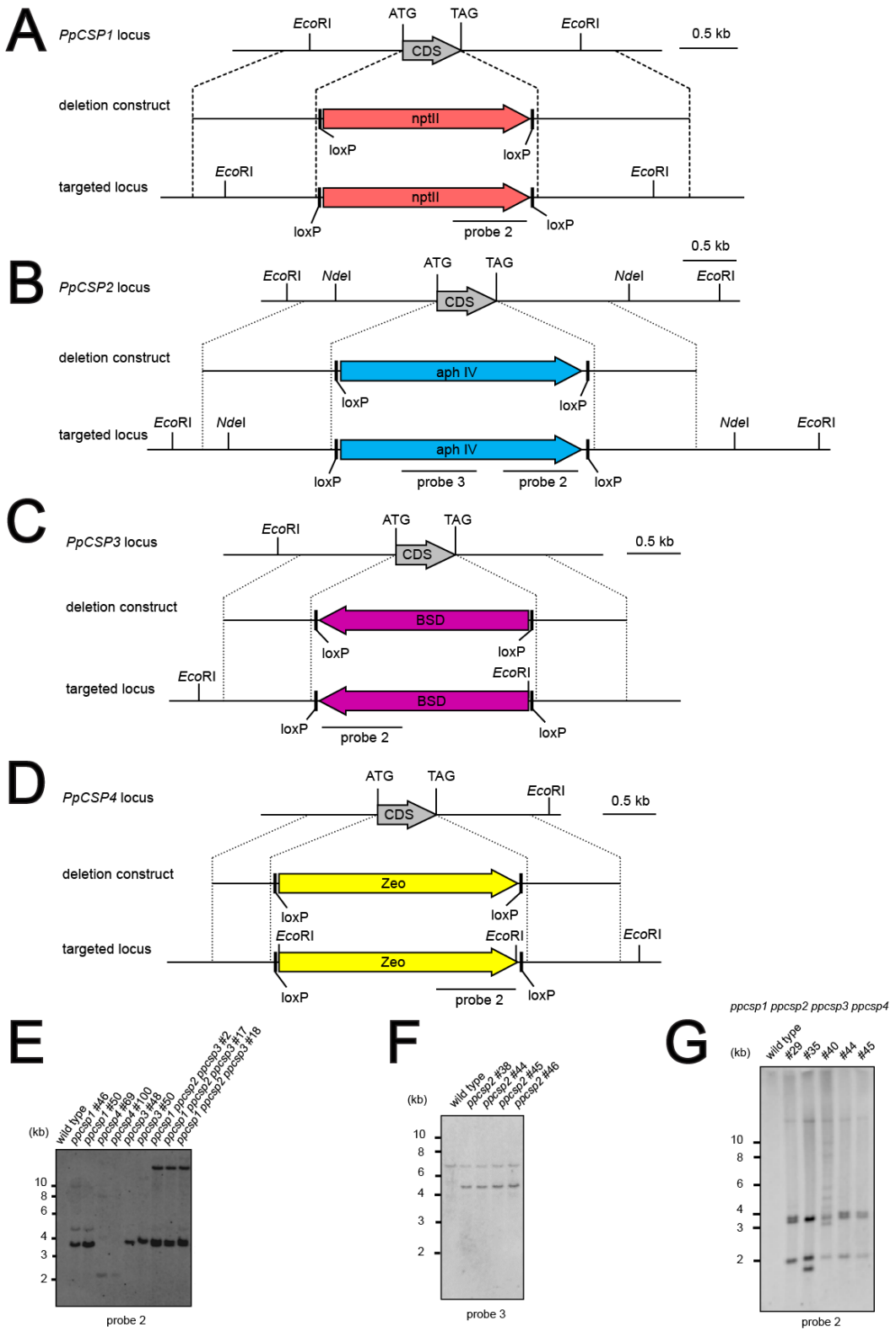
A
PpCSP1 locus
EcoRI
ATG
TAG
EcoRI
0.5 kb
CDS
deletion construct
nptII
loxP
loxP
targeted locus
EcoRI
EcoRI
nptII
loxP
probe 2
loxP
B
PpCSP2 locus
EcoRI
NdeI
ATG
TAG
NdeI
EcoRI
0.5 kb
CDS
deletion construct
aph IV
loxP
loxP
targeted locus
EcoRI
NdeI
NdeI
EcoRI
aph IV
loxP
probe 3
probe 2
loxP
C
PpCSP3 locus
EcoRI
ATG
TAG
0.5 kb
CDS
deletion construct
BSD
loxP
loxP
targeted locus
EcoRI
EcoRI
BSD
loxP
probe 2
loxP
D
PpCSP4 locus
ATG
TAG
EcoRI
0.5 kb
CDS
deletion construct
Zeo
loxP
loxP
targeted locus
EcoRI
EcoRI
EcoRI
Zeo
loxP
probe 2
loxP
E
(kb)
wild type
ppcsp1 #46
ppcsp1 #50
ppcsp4 #69
ppcsp4 #100
ppcsp3 #48
ppcsp3 #50
ppcsp1 ppcsp2 ppcsp3 #2
ppcsp1 ppcsp2 ppcsp3 #17
ppcsp1 ppcsp2 ppcsp3 #18
10
8
6
4
3
2
probe 2
F
(kb)
wild type
ppcsp2 #38
ppcsp2 #44
ppcsp2 #45
ppcsp2 #46
10
8
6
4
3
2
probe 3
G
ppcsp1 ppcsp2 ppcsp3 ppcsp4
(kb)
wild type
#29
#35
#40
#44
#45
10
8
6
4
3
2
probe 2

Figure 19. Construction of the *PpCSP* deletion mutants

(A-D) Schematics of constructs targeting the *PpCSP1* (A), *PpCSP2* (B), *PpCSP3* (C), and *PpCSP4* (D) loci. Grey arrows represent the coding regions of *PpCSP1*, *PpCSP2*, *PpCSP3*, and *PpCSP4* in (A-D), respectively. Pink, blue, purple and yellow arrows indicate the neomycin phosphotransferase II expression cassette (nptII) [50], the aminoglycoside phosphotransferase expression cassette (aph IV) [78, 89], the blasticidin S deaminase expression cassette (BSD) [29], and Zeocin resistance cassette (Zeo) [78], respectively. Probes used in (E-G) are indicated. Procedures to make quadruple deletion mutants are described in Materials and Methods.
(E-G) DNA gel-blot analyses of targeted lines. Genomic DNA of wild type, *ppcsp1* (#46 and #50), *ppcsp4* (#69 and #100), *ppcsp3* (#48 and #50), and *ppcsp1 ppcsp2 ppcsp3* (#2, #17, and #18) lines was digested with *Eco*RI and hybridized with probe 2 (E). Genomic DNA of wild type, *ppcsp2* (#38, #44, #45 and #46) lines was digested with *Nde*I and hybridized with probe 3 (F). Genomic DNA of wild type and *ppcsp1 ppcsp2 ppcsp3 ppcsp4* (#29, #35, #44 and #45) lines was digested with *Eco*RI and hybridized with probe 2 (G).

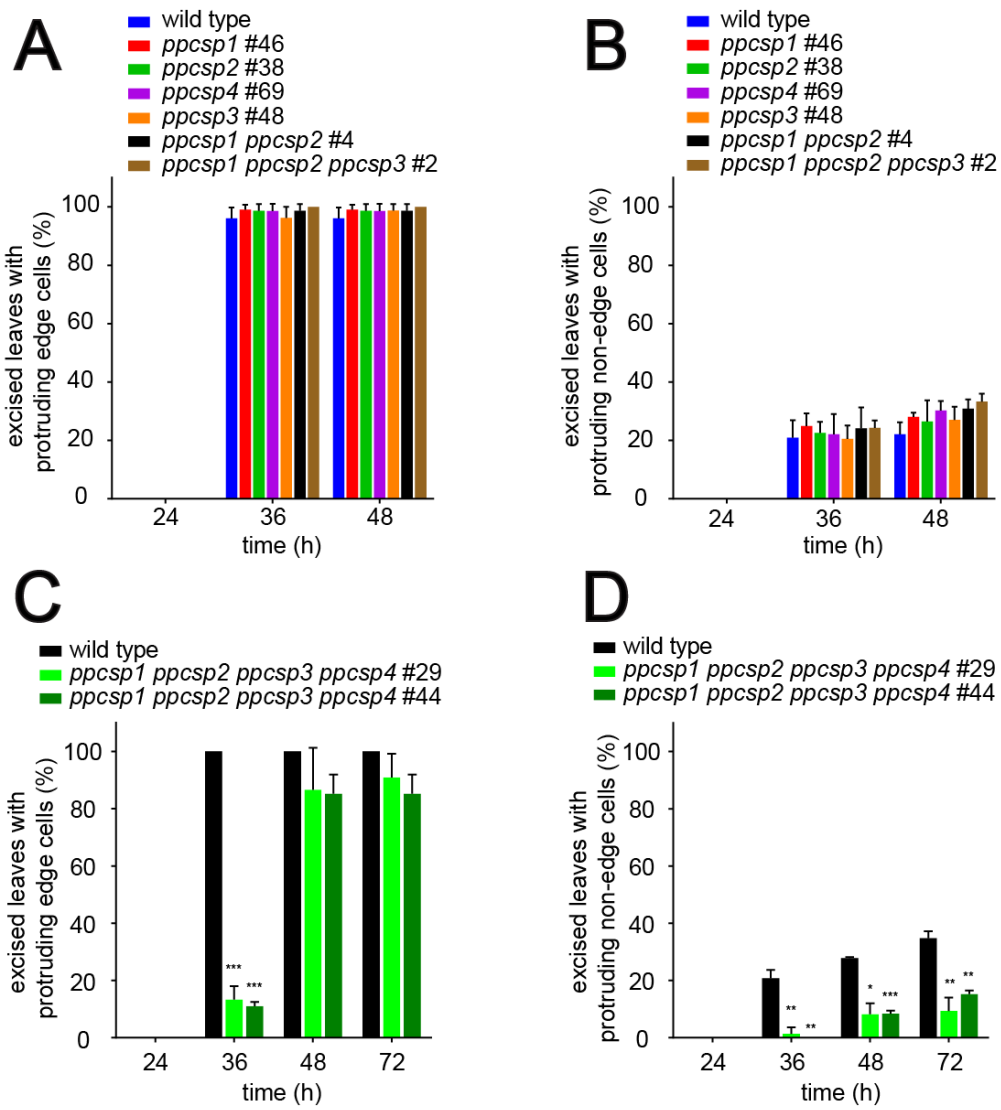
A
wild type
ppcsp1 #46
ppcsp2 #38
ppcsp4 #69
ppcsp3 #48
ppcsp1 ppcsp2 #4
ppcsp1 ppcsp2 ppcsp3 #2
excised leaves with protruding edge cells (%)
100
80
60
40
20
0
24
36
48
time (h)
B
wild type
ppcsp1 #46
ppcsp2 #38
ppcsp4 #69
ppcsp3 #48
ppcsp1 ppcsp2 #4
ppcsp1 ppcsp2 ppcsp3 #2
excised leaves with protruding non-edge cells (%)
100
80
60
40
20
0
24
36
48
time (h)
C
wild type
ppcsp1 ppcsp2 ppcsp3 ppcsp4 #29
ppcsp1 ppcsp2 ppcsp3 ppcsp4 #44
excised leaves with protruding edge cells (%)
100
80
60
40
20
0
***
***
24
36
48
72
time (h)
D
wild type
ppcsp1 ppcsp2 ppcsp3 ppcsp4 #29
ppcsp1 ppcsp2 ppcsp3 ppcsp4 #44
excised leaves with protruding non-edge cells (%)
100
80
60
40
20
0
**
**
*
***
**
**
24
36
48
72
time (h)

Figure 20. Inhibition of reprogramming in quadruple deletion mutants

(A and B) Percentage of excised leaves with protruding edge cells (A) and protruding non-edge cells (B) in wild type, *ppcsp1* #46, *ppcsp2* #38, *ppcsp3* #48, *ppcsp4* #69, *ppcsp1 ppcsp2* #4, and *ppcsp1 ppcsp2 ppcsp3* #2. Twenty leaves were excised from each line. Error bars represent SD of biological triplicates.
(C and D) Percentage of excised leaves of wild type and *ppcsp1 ppcsp2 ppcsp3 ppcsp4* (#29 and #44) with tip growth from edge (C) and non-edge cells (D), respectively. Twenty leaves were excised from each line. Error bars represent SD of biological triplicates. *p < 0.05, **p < 0.01 and ***p < 0.001 by Welch's *t*-test.

gametophores were analyzed. The morphology of protonemata and gametophores of the quadruple deletion mutant and the transcript-increased line could not be distinguished from those of wild type (Figure 21A-21F). Moreover, the duration of cell cycles of protonemata of these lines was measured with time-lapse observation and we could not find any differences (Figure 21G). These results suggest that PpCSP1 does not play a major role in cell cycle progression in protonemata.

When a DNA synthesis inhibitor, aphidicolin, was added to cut leaves, cell cycle reentry was arrested but leaf edge cells are protruded, indicating that cell cycle progression is not required for the reprogramming [29] (Figure 22). To examine whether PpCSP1 regulates reprogramming regardless of cell cycle, the quadruple deletion mutant, *PpCSP1* transcript-increased line, and wild type were treated with aphidicolin and compared their reprogramming phenotype. In the presence of aphidicolin, *ppcsp* quadruple deletion mutant and *PpCSP1* transcript-increased line exhibited attenuated and enhanced reprogramming, respectively as in the absence of the cell-cycle inhibitor (Figure 22). These indicate that PpCSP1 functions in the reprogramming independently of cell cycle progression.

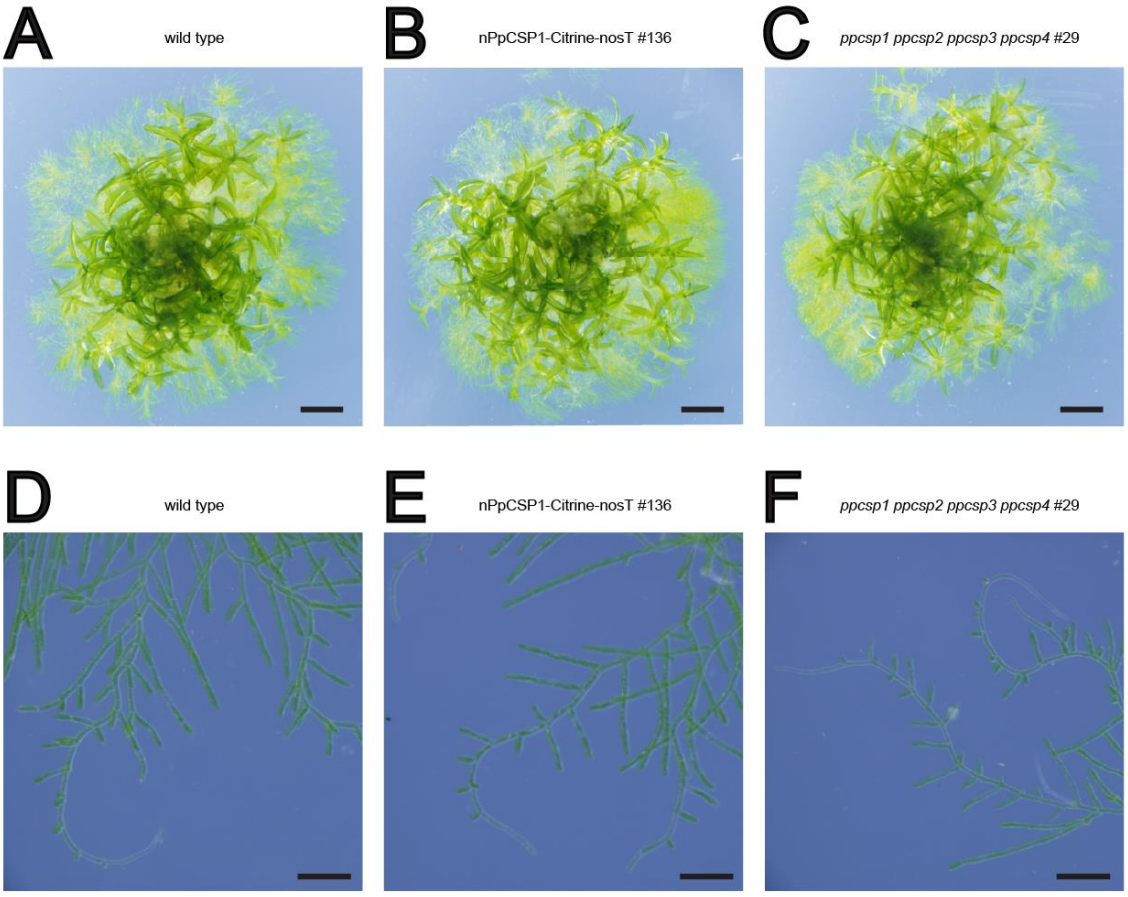
A
wild type
B
nPpCSP1-Citrine-nosT #136
C
ppcsp1 ppcsp2 ppcsp3 ppcsp4 #29
D
wild type
E
nPpCSP1-Citrine-nosT #136
F
ppcsp1 ppcsp2 ppcsp3 ppcsp4 #29

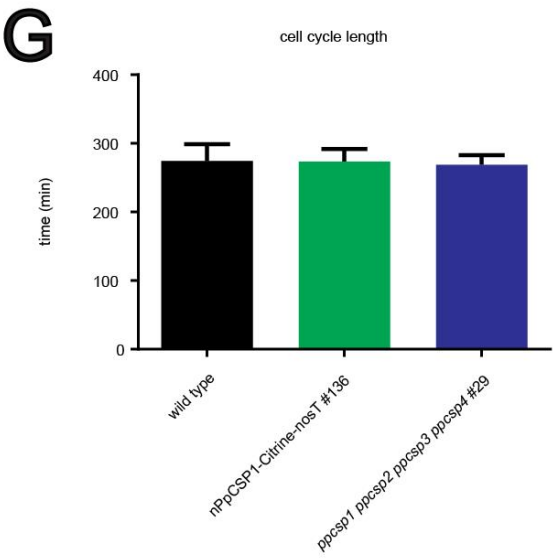
G
cell cycle length
time (min)
400
300
200
100
0
wild type
nPpCSP1-Citrine-nosT #136
ppcsp1 ppcsp2 ppcsp3 ppcsp4 #29

Figure 21. Protonemata and gametophores of the wild type, nPpCSP1-Citrine-nosT line, and quadruple deletion mutant line

(A-F) Representative 4-week-old plants (A-C) and protonemata (D-F) of wild-type (A,D), nPpCSP1-Citrine-nosT #136 (B,E), and *ppcsp1 ppcsp2 ppcsp3 ppcsp4* #29 deletion mutant lines (C,F).
(G) The cell cycle duration of protonemata in the wild type, nPpCSP1-Citrine-nosT #136 line, and *ppcsp1 ppcsp2 ppcsp3 ppcsp4* #29 line. Error bars represent SD (n > 40).
Scale bars represent 2 mm in (A-C) and 200 μm in (D-F).

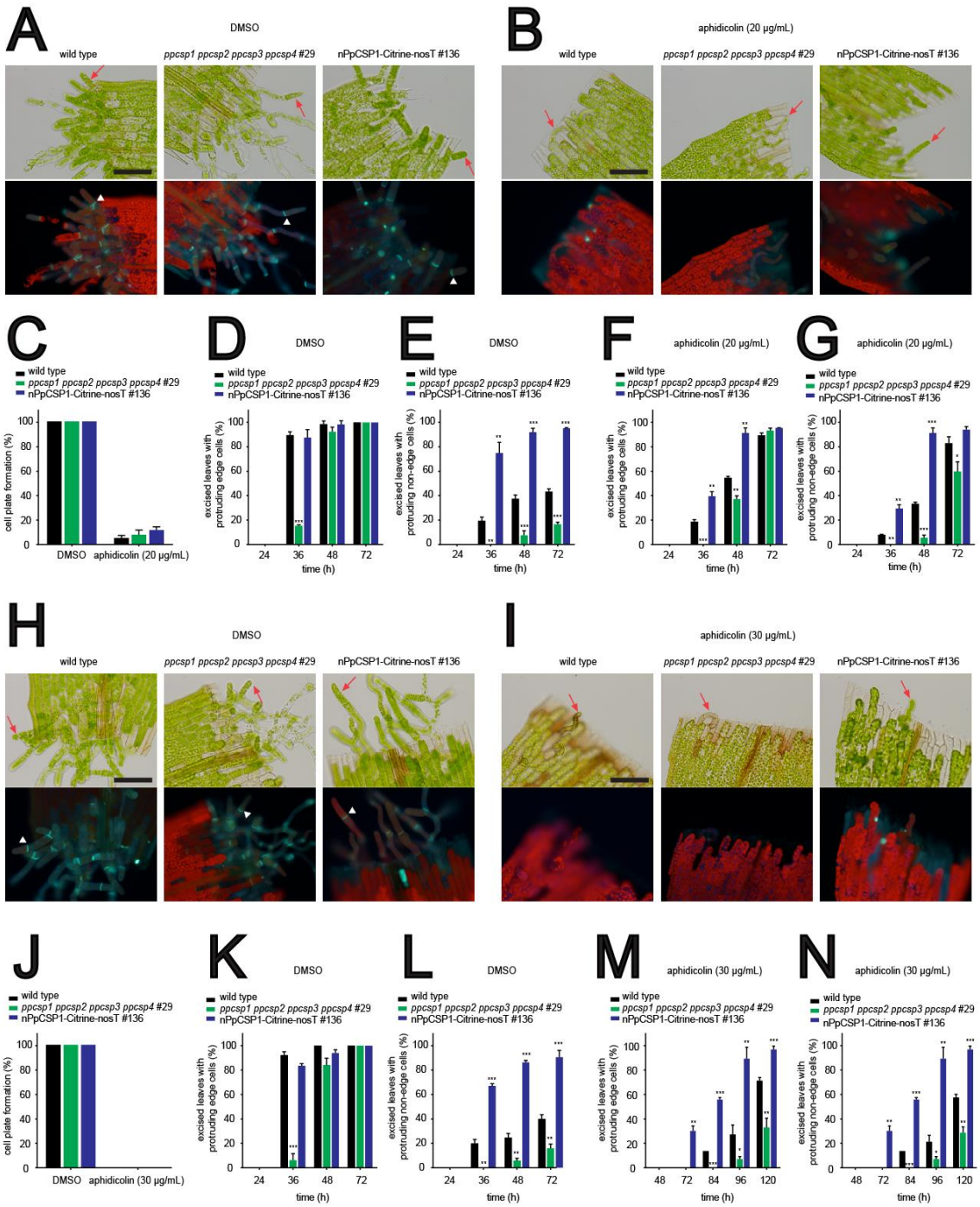
A
DMSO
wild type
ppcsp1 ppcsp2 ppcsp3 ppcsp4 #29
nPpCSP1-Citrine-nosT #136
B
aphidicolin (20 μg/mL)
wild type
ppcsp1 ppcsp2 ppcsp3 ppcsp4 #29
nPpCSP1-Citrine-nosT #136
C
wild type
ppcsp1 ppcsp2 ppcsp3 ppcsp4 #29
nPpCSP1-Citrine-nosT #136
cell plate formation (%)
DMSO
aphidicolin (20 μg/mL)
D
DMSO
wild type
ppcsp1 ppcsp2 ppcsp3 ppcsp4 #29
nPpCSP1-Citrine-nosT #136
excised leaves with protruding edge cells (%)
time (h)
E
DMSO
wild type
ppcsp1 ppcsp2 ppcsp3 ppcsp4 #29
nPpCSP1-Citrine-nosT #136
excised leaves with protruding non-edge cells (%)
time (h)
F
aphidicolin (20 μg/mL)
wild type
ppcsp1 ppcsp2 ppcsp3 ppcsp4 #29
nPpCSP1-Citrine-nosT #136
excised leaves with protruding edge cells (%)
time (h)
G
aphidicolin (20 μg/mL)
wild type
ppcsp1 ppcsp2 ppcsp3 ppcsp4 #29
nPpCSP1-Citrine-nosT #136
excised leaves with protruding non-edge cells (%)
time (h)
H
DMSO
wild type
ppcsp1 ppcsp2 ppcsp3 ppcsp4 #29
nPpCSP1-Citrine-nosT #136
I
aphidicolin (30 μg/mL)
wild type
ppcsp1 ppcsp2 ppcsp3 ppcsp4 #29
nPpCSP1-Citrine-nosT #136
J
wild type
ppcsp1 ppcsp2 ppcsp3 ppcsp4 #29
nPpCSP1-Citrine-nosT #136
cell plate formation (%)
DMSO
aphidicolin (30 μg/mL)
K
DMSO
wild type
ppcsp1 ppcsp2 ppcsp3 ppcsp4 #29
nPpCSP1-Citrine-nosT #136
excised leaves with protruding edge cells (%)
time (h)
L
DMSO
wild type
ppcsp1 ppcsp2 ppcsp3 ppcsp4 #29
nPpCSP1-Citrine-nosT #136
excised leaves with protruding non-edge cells (%)
time (h)
M
aphidicolin (30 μg/mL)
wild type
ppcsp1 ppcsp2 ppcsp3 ppcsp4 #29
nPpCSP1-Citrine-nosT #136
excised leaves with protruding edge cells (%)
time (h)
N
aphidicolin (30 μg/mL)
wild type
ppcsp1 ppcsp2 ppcsp3 ppcsp4 #29
nPpCSP1-Citrine-nosT #136
excised leaves with protruding non-edge cells (%)
time (h)

Figure 22. Reprogramming and cell cycle progression with aphidicolin in the wild type, nPpCSP1-Citrine-nosT line, and quadruple deletion mutant line

(A and B) Bright-field and fluorescent images of excised leaves of the wild type, *ppcsp1 ppcsp2 ppcsp3 ppcsp4* #29 line, and nPpCSP1-Citrine-nosT #136 line incubated with or without 20 μg/mL aphidicolin for 72 h and stained with aniline blue to detect newly synthesized cell plates. Red arrows and white arrowheads indicate some cells with tip growth and newly synthesized cell plates, respectively.
(C) Percentage of excised leaves having at least one cell with cell plate formation (n = 20) after 72-h incubation with 20 μg/mL aphidicolin. Error bars represent SD from biological triplicates.
(D-G) Percentages of excised leaves with protruding edge cells (D,F) and protruding non-edge cells (E,G) without (D,E) or with (F,G) 20 μg/mL aphidicolin. Twenty leaves excised from the wild type, *ppcsp1 ppcsp2 ppcsp3 ppcsp4* #29 line, and nPpCSP1-Citrine-nosT #136 line were used for each analysis. Error bars represent SD from biological triplicates. *p < 0.05, ***p < 0.01, ***p < 0.001 by two-sided Welch's *t*-test.
(H and I) Bright-field and fluorescent images of excised leaves of the wild type, *ppcsp1 ppcsp2 ppcsp3 ppcsp4* #29 line, and nPpCSP1-Citrine-nosT #136 line incubated with or without 30 μg/mL aphidicolin for 72 h (DMSO) or 120 h (aphidicolin) and stained with aniline blue to detect newly synthesized cell plates. Red arrows and white arrowheads indicate some cells with tip growth and newly synthesized cell plates, respectively. For the control experiment with DMSO, we stopped the observation 72 h after the leaf excision, since chloronemata covered the excised leaves and further observation was impossible.
(J) Percentage of excised leaves having at least one cell with cell plate formation (n = 20) after 72-h incubation (DMSO) or 120-h incubation with 30 μg/mL aphidicolin. Error bars represent SD from biological triplicates.
(K-N) Percentages of excised leaves with protruding edge cells (K,M) and protruding non-edge cells (L,N) without (K,L) or with (M,N) 30 μg/mL aphidicolin. Twenty leaves excised from the wild type, *ppcsp1 ppcsp2 ppcsp3 ppcsp4* #29 line, and nPpCSP1-Citrine-nosT #136 line were used for each analysis. Error bars represent SD from biological triplicates. *p < 0.05, ***p < 0.01, ***p < 0.001 by two-sided Welch's *t*-test.
Scale bars represent 100 μm in (A,B,H,I).

2.4 DISCUSSION

A model for PpCSP1 function in the reprogramming

This study revealed that PpCSP1 functions in the enhancement of the reprogramming of differentiated cells to stem cells in Physcomitrella. In the leaf cut system, PpCSP1-Citrine signals specifically increased in leaf cells facing the cut just after excision and increased continuously during the reprogramming process (Figures 5-8). This suggests that the involvement of PpCSP1 in the reprogramming from differentiated leaf cells to protonema apical stem cells. To further analyze the expression behavior of *PpCSP1* during the reprogramming, a dual reporter line (PpCSP1pro:LUC nPpCSP1-Citrine-3'UTR) was produced, which could be used to simultaneously monitor promoter activity and protein levels at the single-cell level (Figure 7). Quantitative analyses of the promoter activity and protein levels indicate that they are overall similar, but certain differences existed: The promoter activity reached maximum approximate 12 hours after cutting, and was maintained with fluctuations, while the protein levels kept increasing during the reprogramming (Figures 7 and 8). These data suggest the potential involvement of post-transcriptional regulation in the *PpCSP1* expression during the reprogramming. In addition, *PpCSP1* was negatively regulated via its 3' UTR. 5'-DGE analysis was performed to compare the position of the 5'-end and the amount of *PpCSP1* transcripts in the nPpCSP1-Citrine-3'UTR and

nPpCSP1-Citrine-nosT lines. Both the rate of full-length transcripts and the transcript amount of *PpCSP1* were higher in the nPpCSP1-Citrine-nosT line than in the nPpCSP1-Citrine-3'UTR line, suggesting the degradation function of the 3'UTR (Figure 9). This was further confirmed by the study of sGFP intensity in the EF1αpro:sGFP-nosT and EF1αpro:sGFP-3'UTR lines, where sGFP levels were weaker in the EF1αpro:sGFP-3'UTR line than in EF1αpro:sGFP-nosT line in all leaf cells examined during the reprogramming (Figures 11 and 12). Analysis of deletion series of the 3' UTR suggest that several different regions in the 3' UTR serve as targets for the negative regulation (Figure 13). Future studies to find factors regulating the 3' UTR function will be needed to understand the regulation mechanism of the *PpCSP1* expression. To understand the function of PpCSP1 in the reprogramming, the gain-of-function and loss-of-function analyses were performed. Increased transcript levels of *PpCSP1* enhanced the reprogramming of non-edge cells in nPpCSP1-Citrine-nosT line, and the *ppcsp* quadruple deletion mutant exhibited attenuated reprogramming (Figures 14-19). These data indicate that PpCSP1 is a positive regulator that functions in enhancing the reprogramming in Physcomitrella.

Based upon the results in this study, a model for the function of *PpCSP1* in the cellular reprogramming of Physcomitrella was proposed (Figure 23). *PpCSP1* mRNA is weakly transcribed and degraded through regulatory elements localized in the 3' UTR in all

leaf cells (Figures 9-13). Subsequent to excision, a wound signal induces promoter activity and overcomes the degradation, which results in an increase in transcript and protein levels (Figures 5-8). The increase of promoter activity is strong enough for reprogramming in edge cells but not in non-edge cells. Since some edge-cells are not reprogrammed (Figures 5-8), another unidentified factor (X) must be necessary for uniform edge cell reprogramming. Furthermore, since some reprogramming still occurs in the *ppcsp* quadruple deletion line (Figure 20C), another inductive pathway occurring independent of PpCSP1 must exist (Figure 23). In the nPpCSP1-Citrine-nosT and PpCSP1pro-PpCSP1-Citrine lines, without repression mediated by the 3' UTR, PpCSP1 expression increases and triggers reprogramming in non-edge cells (Figures 14-17).

In addition, PpCSP1 was predominantly expressed in protonema apical stem cells in Physcomitrella (Figure 3). This suggest that the involvement of PpCSP1 in stem-cell maintenance. However, there is no obvious phenotype in apical cells in the *PpCSP1* transcript-increased line and the *ppcsp* quadruple deletion line. Future experiments to study the activity of apical stem cells under different conditions might help to reveal PpCSP1 function in regular stem-cell system.

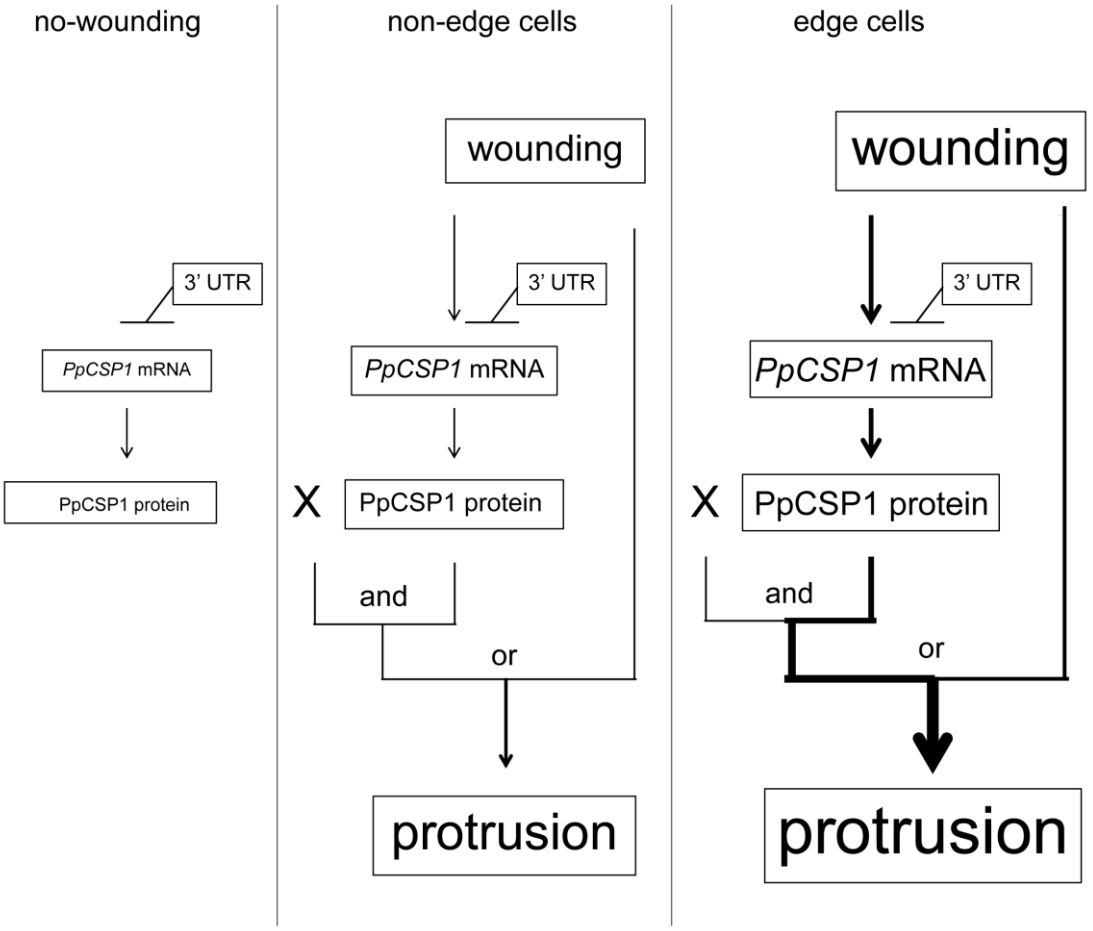

Figure 23. A model for PpCSP1 function in the reprogramming

Hypothetical model of the function of PpCSP1 in the reprogramming. The 3' UTR represses PpCSP1 expression in both edge and non-edge cells. Signals from wounding are capable of overriding the repression effectively increasing PpCSP1 expression, resulting in activation of the reprogramming process.

3. GENERAL DISCUSSION

PpCSP1/Lin28 is a common factor enhancing the reprogramming in land plants and metazoa

By BLASTP searches to nr and metazoan databases using the amino-acid sequence of PpCSP1 as a query, PpCSP1 was found to share highest amino-acid sequence similarity with Lin28 in the genomes of *C. elegans*, drosophila, mouse, and human. In addition, in metazoa, only Lin28 family proteins (Figure 4) share the domain structure with PpCSP1; one CSD and two zinc-finger domains. These data suggest that the closely related protein to PpCSP1 in metazoa is Lin28. *PpCSP1* is involved in the reprogramming of differentiated cells to stem cells in Physcomitrella as its mammalian closely related gene *Lin28*. Both *PpCSP1* and *Lin28* are dispensable for reprogramming; rather function in the enhancement of reprogramming: *Lin28* is dispensable for iPSC formation and promotes the maturation of iPSCs [11, 12, 90], although *Lin28* participates in the effective iPSC reprogramming from human fibroblast cell [5]. In the *ppcsp* quadruple deletion line of Physcomitrella, reprogramming was attenuated in edge cells but was not completely arrested (Figure 20), while non-edge cells were effectively reprogrammed in the *PpCSP1* transcript-increased lines (Figures 14-17). However, the molecular mechanisms underlying *PpCSP1* and *Lin28* regulation appear to be different. Lin28 binds to precursors of miRNA *let-7* and inhibits its

processing [43-45], while *let-7* leads to the degradation of *Lin28* transcripts [43]. Therefore, this negative feedback loop functions as a bistable switch to regulate the cell fate [43]. Although regulation of *PpCSP1* transcripts was found to be mediated by its 3' UTR, miRNA binding sites were not found in this region and *let-7* homologs were not in the Physcomitrella genome. Furthermore, the degradation of *PpCSP1* transcripts is not specific to the differentiated cells (Figure 11). The activation of the *PpCSP1* promoter in the reprogramming cells results in the increase of *PpCSP1* transcripts (Figure 23).

Multicellularity with stem cells has evolved independently in land plant and metazoan lineages and the molecular mechanisms underlying reprogramming appear to differ between these lineages [1-4]. Nevertheless, this study showed that closely related genes encoding CSD proteins, PpCSP1 and Lin28, are involved in the reprogramming, although their orthology was not clear (Figure 4). Therefore, it is an open question whether PpCSP1 and Lin28 have evolved from a common gene or different genes of the last common ancestor.

CSD is highly conserved in bacteria, land plants and metazoa [36, 37], but the biochemical function of CSD in the reprogramming is unknown. In *Escherichia coli*, CSPs function as RNA chaperones that destabilize secondary structures in RNA [39, 40]. Wheat cold shock domain protein 1 (WCSP1) has nucleic acid binding activity, antitermination

activity, and dsDNA melting activity [35]. Ectopic expression of WCSP1 in *E. coli* CSP deletion mutant could complement its cold-sensitive phenotype [35], suggesting that the CSP function as RNA chaperone in response to cold stress is the ancestral function of CSP between bacteria and land plants. Arabidopsis CSPs (AtCSPs) also function in the stress response and regular development [34, 91-96]. However, no report has shown that CSPs function in stem cell establishment/maintenance or reprograming in flowering plants. GUS reporter analysis showed that AtCSPs are expressed in shoot and root meristem harboring stem cells [34, 94-96]. These suggest that AtCSPs may play a role in stem cell regulation in *Arabidopsis*. It will be a future challenge to investigate the biochemical functions of CSD within PpCSPs and AtCSPs in reprogramming.

PpCSP1-Citrine signals localized at the phragmoplast when the reprogrammed leaf cells divide (Figure 6). The signals were maintained in the reprogrammed chloronema apical stem cells and diminished in the successive cell divisions, although the diminished signals were maintained in chloronema apical stem cells (Figure 6). In addition, PpCSP1 was expressed in both stem cells and proliferating non-stem cells in gametophore apices (Figure 5D). These results suggest that PpCSP1 is involved in the cell cycle regulation during or after the reprogramming, as Lin28 promotes cell-cycle regulators and coordinates proliferative growth [68, 69]. However, increase and decrease of PpCSP1 levels in

nPpCSP1-Citrine-nosT and quadruple deletion mutant lines, respectively did not change the duration of cell cycles in protonema apical stem cells (Figure 21G). Moreover, aphidicolin blocked cell cycle reentry, nevertheless cells facing the cut protruded without dividing, indicating that the reprogramming does not require cell cycle progression. In the presence of aphidicolin, *PpCSPs* quadruple deletion mutant and *PpCSP1* transcript-increased line exhibited attenuated and enhanced reprogramming, respectively (Figure 22). These results indicate that PpCSP1 plays a role in the reprogramming. It is a future question whether PpCSP1 functions in the cell cycle regulation during the reprogramming.

In human cells, overexpression of Lin28 with a set of pluripotency associated transcription factors Oct4, Sox2, and Nanog promotes reprogramming of fibroblast cells into iPSCs [5]. In addition to *let-7*, Lin28 binds to various mRNAs including approximately 50% of the human transcripts with recognitions of GGAG or GGAG-like motif [46-48]. Future studies are warranted to investigate more detailed *PpCSP1* regulatory networks in order to find molecular mechanisms underlying the similar functions between PpCSP1 and Lin28.

Perspective

The present study provides a new insight into evolutionary conserved proteins that function in reprogramming. PpCSP1/Lin28 are the first common stem-cell inducing factor to be

shared between land plants and metazoa. However, the molecular mechanism of how PpCSP1 reprogram differentiated cell to stem cell is still not clear. For the future prospective, there are several approaches to deepen the understanding of PpCSP1 functions. First, transcriptome analysis of wild type, the *PpCSP1* transcript-increased line, and the quadruple deletion mutant line will provide useful information of downstream candidates in PpCSP1 pathway. For example, It is worth to analyze whether PpCSP1 regulates conserved metabolic oxidative enzymes to connect the particular metabolic states of stem cells and pluripotency, which was found in Lin28 function in mice [49]. Second, due to the presence of the CSD and zinc-finger domains, it is plausible that PpCSP1 functions as an RNA-binding protein to regulate mRNA maturation, stability, or translation in the cytosol in a manner similar to that reported for other CSPs [35, 36]. The key question will be to identify PpCSP1 targets mRNA. With cross-linking immunoprecipitation (CLIP), it was found that PpCSP1 binds to mRNA in vivo (Figure 24). It may help to know the molecular function of PpCSP1 if mRNAs obtained from CLIP are sequenced using next generation sequencer (CLIP-seq) [63, 64] to know its direct targets in Physcomitrella. By exchanging the motifs to those of Lin28, the conservation of the biochemical functions between Lin28 and PpCSP1 will be analyzed. In addition, protein interactome analysis could give more information how PpCSP1 protein-RNA complex influences target mRNA fate, such as maturation, stability, localization,

and translation. Approaches above will provide molecular mechanisms underlying PpCSP1-mediated reprogramming, of which the comparison to those of Lin28 sheds light on the evolution of reprogramming in land plant and metazoan lineages.

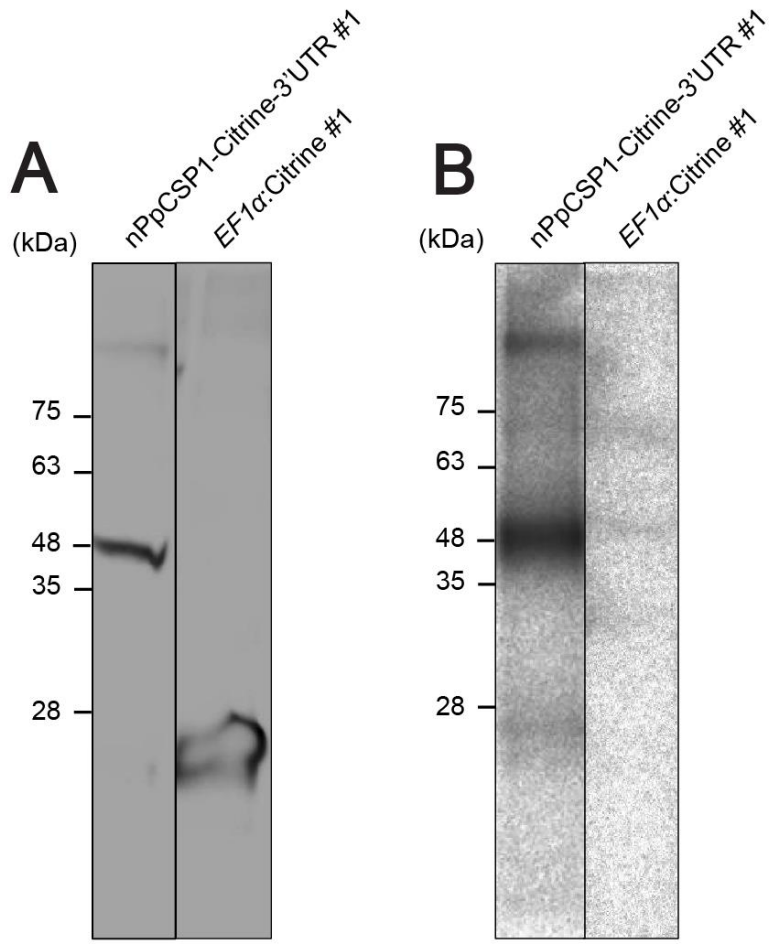

Figure 24. PpCSP1 binds to RNA in vivo

(A) Immunoblot analysis of PpCSP1-Citrine fusion protein and Citrine protein in nPpCSP1-Citrine-3'UTR #1 and EF1αpro:Citrine #1 lines, respectively. Anti-GFP antibody was used to recognize the protein.
(B) Autoradiograph of the signals of ^{32}P-labeled RNAs, which were immunoprecipitated with PpCSP1-Citrine fusion protein and Citrine protein in nPpCSP1-Citrine-3'UTR #1 and EF1αpro:Citrine #1 lines, respectively. ^{32}P -γ-ATP was used to label RNAs.

Table 1. Primer sequences used for RT-qPCR and plasmid construction

Primers used for RT-qPCR

Gene name		Sequence
PpCSP1	(F)	5’-GCCTGCGAGTCCGTCTTTC-3’
	(R)	5’-GGCGCAAAGATCCCAACA-3’
PpCSP2	(F)	5’-CTCCTGGTACTGTGAATAGTCGAGT-3’
	(R)	5’-GTCTCCTTCGCCTCCGTGCT-3’
PpCSP3,4	(F)	5’-CCGTCTTGCCTTTAGGTCCTTCTTT-3’
	(R)	5’-TCGCTCCCTCTTCCGCCATG-3’
sGFP	(F)	5’-GTCCGCCCTGAGCAAAGA-3’
	(R)	5’-TCCAGCAGGACCATGTGATC-3’
TUA1	(F)	5’-CGTAGGAGGGACCAGTTTGG-3’
	(R)	5’-TGCATTCATCCCCGAGTCA-3’

Primers used for probe amplification

Probe name		Sequence
Probe 1	(F)	5’-GCTGTCGGTCTTCGCCTGCG-3’
	(R)	5’-CCTCGACCTCCTCCATCGCC-3’
Probe 2	(F)	5’-TGAAATCACCAGTCTCTCTCTACAA-3’
	(R)	5’-GTTTTGATCTTGAAAGATCTTTTATCTTTAGA-3’
Probe 3	(F)	5’-ATATGAAGAAGCCTGAACTCA-3’
	(R)	5’-CTATTCCTTTGCCCTAGGACGAGTGCT-3’

Primers used for plasmid construction

Construct		Sequence
nPpCSP1-Citrine-nosT	5'(F)	5'-TCTCTCGAGAGCTGAGCTGGAATCGGG-3'
	5'(R)	5'-AGAATCGATGGAAGCGGCTGCAGGAGTG-3'
	3'(F)	5'-TCTACTAGTTAGGTGCTTCCGAGTAG-3'
	3'(R)	5'-AGAGCGGCCGCAAAAATCATCTACTCG-3'
pAK101	(F)	5'- GCATCTAGAGAGTTTTTGCAGGTAATCGAAGGTT -3'
	(R)	5'-GGGAAGCTTAAAAGCCTATACTGTACTTAACTTGATTG -3'
PpCSP1:LUC	(F)	5'-CACCAACGATTGTGCGACCATGCACACCGA-3'
	(R)	5'-CATAGCTGCTGCTGCGCCTCTCT-3'
EF1αpro:sGFP-nosT	(F)	5'-CACCATGGTGAGCAAGGGCGAGGAGCTGTTC-3'
	(R)	5'-TTACTTGTACAGCTCGTCCATGCC-3'
EF1αpro:sGFP-3'UTR	(F)	5'- CACCATGGTGAGCAAGGGCGAGGAGCTGTTC-3'
	(R)	5'-AAGGGCCCTCATCTACTCGAATGATTGCCTTCC-3'
3' UTR-623	(F)	5'-AAGGGCCCGTGCTTCCGAGTAGAAACAATTTTTCAAC-3'
	(R)	5'-AAGGGCCCTCATCTACTCGAATGATTGCCT TCC-3'
3' UTR-500	(R)	5'-AAGGGCCCTGACACAACATAAACCCTTCT CG-3'
3' UTR-400	(R)	5'-AAGGGCCCCATCCATCGCGGAGGAGCT-3'
3' UTR-300	(R)	5'-AAGGGCCCAAAGCAAACTTCTGCATACTACATTATAC C-3'
3' UTR-200	(R)	5'-AAGGGCCCAAAAAACAAAGTCAAGCAGAG CACTAC-3'
PpCSP1pro:PpCSP1-Citri	(F)	5'-AATCCTCGAGCCCGGGAGCTTTGGATTCCATTGCACA C-3'
	(R)	5'- AATCTGTACACTAGGAAGCGGCTGCAGG-3'
ppcsp1	5'(F)	5'-TCTCTCGAGCATGTCTAAAGCTAACATCACC ACTG-3'
	5'(R)	5'-AGAATCGATAGCTGCTGCTGCGCCTCTCTG CCTTAC-3'
	3'(F)	5'-TCTCATATGGTGCTTCCGAGTAGAAACAATT TTTC-3'
	3'(R)	5'-AGAGGATCCCATCAATATACTCCTTGATGGC AGTC-3'
ppcsp2	5'(F)	5'-TCTCTCGAGGTGTAGTGCTGTTGTAATTCT CCTTG-3'
	5'(R)	5'-AGAATCGATAGCTCCCGACTCGACTATTCA CAGTAC-3'
	3'(F)	5'-TCTGGATCCTTGCTTCACTAGAGAGGCAAT GGTC-3'
	3'(R)	5'-AGAGAGCTCTGTATCCGTAAGGACGGATTA CTCTC-3'
ppcsp3	5'(F)	5'-AGGCTCGAGAAGCCAACGGTAAATCCCGA TAA-3'
	5'(R)	5'-CGCATCGATTGCTGCTGCGCCTCTCTGCG G-3'
	3'(F)	5'-TCTCCCGGGGCGTTTCCGAGTAGAAGC-3'
	3'(R)	5'-TCTCCGCGGCCACCTCTTCATCCCAATG-3'
ppcsp4	5'(F)	5'-TCTCCGCGGAATGGGTTCCCAACCAGC-3'
	5'(R)	5'-TCTCATATGTGCTGCTGCGCCTCTCTGC-3'
	3'(F)	5'-TCTATCGATGCGTTTCCGAGTAGAAGC-3'
	3'(R)	5'-TCTCTCGAGCCACCTCTTCATCCCAATG-3'

ACKNOWLEDGEMENTS

I am deeply indebted to Professor Mitsuyasu Hasebe for his generous supports, advice, and helpful discussion. Professor Mitsuyasu Hasebe provides outstanding research conditions and enables me to work on this project. I am grateful to Dr. Yosuke Tamada for helpful discussion, and experiment support for my project and thesis. Dr. Yosuke Tamada taught me many research skills for the moss *Physcomitrella patens* which is a totally new material for me when I joined this lab. This work would have not been possible without their understandings and supports.

I sincerely wish to thank many colleagues for collaborations works. Ms. Kari Thompson and Dr. Dale Karlson for initiating this project to study CSP function in the moss *Physcomitrella patens.* Dr. Yusuke Sako and Dr. Yoshikatsu Sato for their excellent work of transgenic line constructions and imaging. Dr. Akihiro Imai and Dr. Philip N. Benfey for Luciferase imaging. Dr. Minoru Kubo and Dr. Yuji Hiwatashi for providing materials. Dr. Yukiko Kabeya for technical support. Dr. Takashi Murata for imaging analysis. Dr. Tomoaki Nishiyama for bioinformatics.

I would like to thank all members in the lab of Professor Mitsuyasu Hasebe and the ERATO Reprogramming Evolution Project for useful discussions and technical support; Dr. Shu-Hsing Wu, Dr. Shih-Long Tu, Dr. Chunli Chen, Dr. Xiangdong Fu, Dr. Yan Sun, and Dr.

Changwei Shao for helpful discussions. I also thank the Functional Genomics Facility, Model Plant Research Facility, Spectrography and Bioimaging Facility, and the Data Integration and Analysis Facility of National Institute for Basic Biology for their technical support.

I also would like to thank The Ministry of Education, Culture, Sports, Science and Technology to provide scholarship during my PhD course.

Finally, I thank my family and friends for many supports.

REFERENCES

1. Sánchez Alvarado, A., and Yamanaka, S. (2014). Rethinking differentiation: stem cells, regeneration, and plasticity. Cell *157*, 110-119.
2. Heidstra, R., and Sabatini, S. (2014). Plant and animal stem cells: similar yet different. Nat. Rev. Mol. Cell Biol. *15*, 301-312.
3. Sugimoto, K., Gordon, S.P., and Meyerowitz, E.M. (2011). Regeneration in plants and animals: dedifferentiation, transdifferentiation, or just differentiation? Trends Cell Biol. *21*, 212-218.
4. Birnbaum, K.D., and Sánchez Alvarado, A. (2008). Slicing across kingdoms: regeneration in plants and animals. Cell *132*, 697-710.
5. Yu, J., Vodyanik, M.A., Smuga-Otto, K., Antosiewicz-Bourget, J., Frane, J.L., Tian, S., Nie, J., Jonsdottir, G.A., Ruotti, V., Stewart, R., Slukvin, II, and Thomson, J.A. (2007). Induced pluripotent stem cell lines derived from human somatic cells. Science *318*, 1917-1920.
6. Poss, K.D. (2010). Advances in understanding tissue regenerative capacity and mechanisms in animals. Nat. Rev. Genet. *11*, 710-722.
7. Gurdon, J.B., Elsdale, T.R., and Fischberg, M. (1958). Sexually mature individuals of Xenopus laevis from the transplantation of single somatic nuclei. Nature *182*, 64-65.
8. Stadtfeld, M., and Hochedlinger, K. (2010). Induced pluripotency: history, mechanisms, and applications. Genes & Development *24*, 2239-2263.
9. Weintraub, H., Tapscott, S.J., Davis, R.L., Thayer, M.J., Adam, M.A., Lassar, A.B., and Miller, A.D. (1989). Activation of muscle-specific genes in pigment, nerve, fat, liver, and fibroblast cell lines by forced expression of MyoD. Proc. Natl. Acad. Sci. USA *86*, 5434-5438.
10. Tapscott, S.J., Davis, R.L., Thayer, M.J., Cheng, P.F., Weintraub, H., and Lassar, A.B. (1988). MyoD1: a nuclear phosphoprotein requiring a Myc homology region to convert fibroblasts to myoblasts. Science *242*, 405-411.
11. Takahashi, K., and Yamanaka, S. (2006). Induction of pluripotent stem cells from mouse embryonic and adult fibroblast cultures by defined factors. Cell *126*, 663-676.
12. Takahashi, K., Tanabe, K., Ohnuki, M., Narita, M., Ichisaka, T., Tomoda, K., and Yamanaka, S. (2007). Induction of pluripotent stem cells from adult human fibroblasts by defined factors. Cell *131*, 861-872.
13. Aichinger, E., Kornet, N., Friedrich, T., and Laux, T. (2012). Plant stem cell niches. Annu. Rev. Plant Biol. *63*, 615-636.
14. Lau, S., Slane, D., Herud, O., Kong, J., and Jurgens, G. (2012). Early embryogenesis

in flowering plants: setting up the basic body pattern. Annu. Rev. Plant Biol. *63*, 483-506.

15. Petricka, J.J., Winter, C.M., and Benfey, P.N. (2012). Control of Arabidopsis root development. Annu. Rev. Plant Biol. *63*, 563-590.
16. Sena, G., Wang, X., Liu, H.Y., Hofhuis, H., and Birnbaum, K.D. (2009). Organ regeneration does not require a functional stem cell niche in plants. Nature *457*, 1150-1153.
17. Steward, F., Mapes, M.O., and Mears, K. (1958). Growth and organized development of cultured cells. II. Organization in cultures grown from freely suspended cells. Am. J. Bot., 705-708.
18. Sugimoto, K., Jiao, Y., and Meyerowitz, E.M. (2010). Arabidopsis regeneration from multiple tissues occurs via a root development pathway. Dev. Cell *18*, 463-471.
19. Ikeuchi, M., Sugimoto, K., and Iwase, A. (2013). Plant callus: mechanisms of induction and repression. Plant Cell *25*, 3159-3173.
20. Fan, M., Xu, C., Xu, K., and Hu, Y. (2012). LATERAL ORGAN BOUNDARIES DOMAIN transcription factors direct callus formation in Arabidopsis regeneration. Cell Res. *22*, 1169-1180.
21. Iwase, A., Mitsuda, N., Koyama, T., Hiratsu, K., Kojima, M., Arai, T., Inoue, Y., Seki, M., Sakakibara, H., Sugimoto, K., and Ohme-Takagi, M. (2011). The AP2/ERF transcription factor WIND1 controls cell dedifferentiation in Arabidopsis. Curr. Biol. *21*, 508-514.
22. Banno, H., Ikeda, Y., Niu, Q.W., and Chua, N.H. (2001). Overexpression of Arabidopsis ESR1 induces initiation of shoot regeneration. Plant Cell *13*, 2609-2618.
23. Wildwater, M., Campilho, A., Perez-Perez, J.M., Heidstra, R., Blilou, I., Korthout, H., Chatterjee, J., Mariconti, L., Gruissem, W., and Scheres, B. (2005). The RETINOBLASTOMA-RELATED gene regulates stem cell maintenance in Arabidopsis roots. Cell *123*, 1337-1349.
24. Cove, D., Bezanilla, M., Harries, P., and Quatrano, R. (2006). Mosses as model systems for the study of metabolism and development. Annu. Rev. Plant Biol. *57*, 497-520.
25. Rensing, S.A., Lang, D., Zimmer, A.D., Terry, A., Salamov, A., Shapiro, H., Nishiyama, T., Perroud, P.F., Lindquist, E.A., Kamisugi, Y., Tanahashi, T., Sakakibara, K., Fujita, T., Oishi, K., Shin, I.T., Kuroki, Y., Toyoda, A., Suzuki, Y., Hashimoto, S., Yamaguchi, K., Sugano, S., Kohara, Y., Fujiyama, A., Anterola, A., Aoki, S., Ashton, N., Barbazuk, W.B., Barker, E., Bennetzen, J.L., Blankenship, R., Cho, S.H., Dutcher, S.K., Estelle, M., Fawcett, J.A., Gundlach, H., Hanada, K., Heyl,

A., Hicks, K.A., Hughes, J., Lohr, M., Mayer, K., Melkozernov, A., Murata, T., Nelson, D.R., Pils, B., Prigge, M., Reiss, B., Renner, T., Rombauts, S., Rushton, P.J., Sanderfoot, A., Schween, G., Shiu, S.H., Stueber, K., Theodoulou, F.L., Tu, H., Van de Peer, Y., Verrier, P.J., Waters, E., Wood, A., Yang, L., Cove, D., Cuming, A.C., Hasebe, M., Lucas, S., Mishler, B.D., Reski, R., Grigoriev, I.V., Quatrano, R.S., and Boore, J.L. (2008). The *Physcomitrella* genome reveals evolutionary insights into the conquest of land by plants. Science *319*, 64-69.

26. Schaefer, D., Zryd, J.P., Knight, C.D., and Cove, D.J. (1991). Stable transformation of the moss Physcomitrella patens. Mol. Genet. Genomics *226*, 418-424.
27. Schaefer, D.G., and Zryd, J.P. (1997). Efficient gene targeting in the moss Physcomitrella patens. Plant J. *11*, 1195-1206.
28. Kofuji, R., and Hasebe, M. (2014). Eight types of stem cells in the life cycle of the moss *Physcomitrella patens*. Curr. Opin. Plant Biol. *17*, 13-21.
29. Ishikawa, M., Murata, T., Sato, Y., Nishiyama, T., Hiwatashi, Y., Imai, A., Kimura, M., Sugimoto, N., Akita, A., Oguri, Y., Friedman, W.E., Hasebe, M., and Kubo, M. (2011). Physcomitrella cyclin-dependent kinase A links cell cycle reactivation to other cellular changes during reprogramming of leaf cells. Plant Cell *23*, 2924-2938.
30. Nishiyama, T., Miyawaki, K., Ohshima, M., Thompson, K., Nagashima, A., Hasebe, M., and Kurata, T. (2012). Digital gene expression profiling by 5'-end sequencing of cDNAs during reprogramming in the moss *Physcomitrella patens*. PLoS One *7*, e36471.
31. Sakakibara, K., Reisewitz, P., Aoyama, T., Friedrich, T., Ando, S., Sato, Y., Tamada, Y., Nishiyama, T., Hiwatashi, Y., Kurata, T., Ishikawa, M., Deguchi, H., Rensing, S.A., Werr, W., Murata, T., Hasebe, M., and Laux, T. (2014). *WOX13-like* genes are required for reprogramming of leaf and protoplast cells into stem cells in the moss *Physcomitrella patens*. Development *141*, 1660-1670.
32. Goldstein, J., Pollitt, N.S., and Inouye, M. (1990). Major cold shock protein of *Escherichia coli*. Proc. Natl. Acad. Sci. USA *87*, 283-287.
33. Sasaki, K., Kim, M.H., and Imai, R. (2013). Arabidopsis COLD SHOCK DOMAIN PROTEIN 2 is a negative regulator of cold acclimation. New Phytol. *198*, 95-102.
34. Kim, M.H., Sasaki, K., and Imai, R. (2009). Cold shock domain protein 3 regulates freezing tolerance in *Arabidopsis thaliana*. J. Biol. Chem. *284*, 23454-23460.
35. Nakaminami, K., Karlson, D.T., and Imai, R. (2006). Functional conservation of cold shock domains in bacteria and higher plants. Proc. Natl. Acad. Sci. USA *103*, 10122-10127.
36. Graumann, P.L., and Marahiel, M.A. (1998). A superfamily of proteins that contain

the cold-shock domain. Trends Biochem. Sci. *23*, 286-290.

37. Karlson, D., and Imai, R. (2003). Conservation of the cold shock domain protein family in plants. Plant Physiol. *131*, 12-15.

38. Mihailovich, M., Militti, C., Gabaldón, T., and Gebauer, F. (2010). Eukaryotic cold shock domain proteins: highly versatile regulators of gene expression. BioEssays *32*, 109-118.

39. Bae, W., Xia, B., Inouye, M., and Severinov, K. (2000). *Escherichia coli* CspA-family RNA chaperones are transcription antiterminators. Proc. Natl. Acad. Sci. USA *97*, 7784-7789.

40. Xia, B., Ke, H., and Inouye, M. (2001). Acquirement of cold sensitivity by quadruple deletion of the cspA family and its suppression by PNPase S1 domain in *Escherichia coli*. Mol. Microbiol. *40*, 179-188.

41. Ambros, V., and Horvitz, H.R. (1984). Heterochronic mutants of the nematode Caenorhabditis elegans. Science *226*, 409-416.

42. Moss, E.G., Lee, R.C., and Ambros, V. (1997). The cold shock domain protein LIN-28 controls developmental timing in C. elegans and is regulated by the lin-4 RNA. Cell *88*, 637-646.

43. Rybak, A., Fuchs, H., Smirnova, L., Brandt, C., Pohl, E.E., Nitsch, R., and Wulczyn, F.G. (2008). A feedback loop comprising lin-28 and let-7 controls pre-let-7 maturation during neural stem-cell commitment. Nat. Cell Biol. *10*, 987-993.

44. Piskounova, E., Polytarchou, C., Thornton, J.E., LaPierre, R.J., Pothoulakis, C., Hagan, J.P., Iliopoulos, D., and Gregory, R.I. (2011). Lin28A and Lin28B inhibit let-7 microRNA biogenesis by distinct mechanisms. Cell *147*, 1066-1079.

45. Nam, Y., Chen, C., Gregory, R.I., Chou, J.J., and Sliz, P. (2011). Molecular basis for interaction of let-7 microRNAs with Lin28. Cell *147*, 1080-1091.

46. Cho, J., Chang, H., Kwon, S.C., Kim, B., Kim, Y., Choe, J., Ha, M., Kim, Y.K., and Kim, V.N. (2012). LIN28A is a suppressor of ER-associated translation in embryonic stem cells. Cell *151*, 765-777.

47. Wilbert, M.L., Huelga, S.C., Kapeli, K., Stark, T.J., Liang, T.Y., Chen, S.X., Yan, B.Y., Nathanson, J.L., Hutt, K.R., Lovci, M.T., Kazan, H., Vu, A.Q., Massirer, K.B., Morris, Q., Hoon, S., and Yeo, G.W. (2012). LIN28 binds messenger RNAs at GGAGA motifs and regulates splicing factor abundance. Mol. Cell *48*, 195-206.

48. Hafner, M., Max, K.E., Bandaru, P., Morozov, P., Gerstberger, S., Brown, M., Molina, H., and Tuschl, T. (2013). Identification of mRNAs bound and regulated by human LIN28 proteins and molecular requirements for RNA recognition. RNA *19*, 613-626.

49. Shyh-Chang, N., Zhu, H., Yvanka de Soysa, T., Shinoda, G., Seligson, M.T., Tsanov,

K.M., Nguyen, L., Asara, J.M., Cantley, L.C., and Daley, G.Q. (2013). Lin28 enhances tissue repair by reprogramming cellular metabolism. Cell *155*, 778-792.

50. Nishiyama, T., Hiwatashi, Y., Sakakibara, I., Kato, M., and Hasebe, M. (2000). Tagged mutagenesis and gene-trap in the moss *Physcomitrella patens* by shuttle mutagenesis. DNA Res. *7*, 9-17.

51. Griesbeck, O., Baird, G.S., Campbell, R.E., Zacharias, D.A., and Tsien, R.Y. (2001). Reducing the environmental sensitivity of yellow fluorescent protein. Mechanism and applications. J. Biol. Chem. *276*, 29188-29194.

52. Odell, J., Caimi, P., Sauer, B., and Russell, S. (1990). Site-directed recombination in the genome of transgenic tobacco. Mol. Genet. Genomics *223*, 369-378.

53. Kubo, M., Imai, A., Nishiyama, T., Ishikawa, M., Sato, Y., Kurata, T., Hiwatashi, Y., Reski, R., and Hasebe, M. (2013). System for stable beta-estradiol-inducible gene expression in the moss *Physcomitrella patens*. PLoS ONE *8*, e77356.

54. Aoyama, T., Hiwatashi, Y., Shigyo, M., Kofuji, R., Kubo, M., Ito, M., and Hasebe, M. (2012). AP2-type transcription factors determine stem cell identity in the moss *Physcomitrella patens*. Development *139*, 3120-3129.

55. Saitou, N., and Nei, M. (1987). The neighbor-joining method: a new method for reconstructing phylogenetic trees. Mol. Biol. Evol. *4*, 406-425.

56. Banks, J.A., Nishiyama, T., Hasebe, M., Bowman, J.L., Gribskov, M., dePamphilis, C., Albert, V.A., Aono, N., Aoyama, T., Ambrose, B.A., Ashton, N.W., Axtell, M.J., Barker, E., Barker, M.S., Bennetzen, J.L., Bonawitz, N.D., Chapple, C., Cheng, C., Correa, L.G., Dacre, M., DeBarry, J., Dreyer, I., Elias, M., Engstrom, E.M., Estelle, M., Feng, L., Finet, C., Floyd, S.K., Frommer, W.B., Fujita, T., Gramzow, L., Gutensohn, M., Harholt, J., Hattori, M., Heyl, A., Hirai, T., Hiwatashi, Y., Ishikawa, M., Iwata, M., Karol, K.G., Koehler, B., Kolukisaoglu, U., Kubo, M., Kurata, T., Lalonde, S., Li, K., Li, Y., Litt, A., Lyons, E., Manning, G., Maruyama, T., Michael, T.P., Mikami, K., Miyazaki, S., Morinaga, S., Murata, T., Mueller-Roeber, B., Nelson, D.R., Obara, M., Oguri, Y., Olmstead, R.G., Onodera, N., Petersen, B.L., Pils, B., Prigge, M., Rensing, S.A., Riano-Pachon, D.M., Roberts, A.W., Sato, Y., Scheller, H.V., Schulz, B., Schulz, C., Shakirov, E.V., Shibagaki, N., Shinohara, N., Shippen, D.E., Sorensen, I., Sotooka, R., Sugimoto, N., Sugita, M., Sumikawa, N., Tanurdzic, M., Theissen, G., Ulvskov, P., Wakazuki, S., Weng, J.K., Willats, W.W., Wipf, D., Wolf, P.G., Yang, L., Zimmer, A.D., Zhu, Q., Mitros, T., Hellsten, U., Loque, D., Otillar, R., Salamov, A., Schmutz, J., Shapiro, H., Lindquist, E., Lucas, S., Rokhsar, D., and Grigoriev, I.V. (2011). The *Selaginella* genome identifies genetic changes associated with the evolution of vascular plants. Science *332*, 960-963.

57. Kanazawa, T., Era, A., Minamino, N., Shikano, Y., Fujimoto, M., Uemura, T., Nishihama, R., Yamato, K.T., Ishizaki, K., Nishiyama, T., Kohchi, T., Nakano, A., and Ueda, T. (2015). SNARE molecules in *Marchantia polymorpha*: unique and conserved features of the membrane fusion machinery. Plant Cell Physiol.

58. Hori, K., Maruyama, F., Fujisawa, T., Togashi, T., Yamamoto, N., Seo, M., Sato, S., Yamada, T., Mori, H., Tajima, N., Moriyama, T., Ikeuchi, M., Watanabe, M., Wada, H., Kobayashi, K., Saito, M., Masuda, T., Sasaki-Sekimoto, Y., Mashiguchi, K., Awai, K., Shimojima, M., Masuda, S., Iwai, M., Nobusawa, T., Narise, T., Kondo, S., Saito, H., Sato, R., Murakawa, M., Ihara, Y., Oshima-Yamada, Y., Ohtaka, K., Satoh, M., Sonobe, K., Ishii, M., Ohtani, R., Kanamori-Sato, M., Honoki, R., Miyazaki, D., Mochizuki, H., Umetsu, J., Higashi, K., Shibata, D., Kamiya, Y., Sato, N., Nakamura, Y., Tabata, S., Ida, S., Kurokawa, K., and Ohta, H. (2014). *Klebsormidium flaccidum* genome reveals primary factors for plant terrestrial adaptation. Nat. Commun. *5*, 3978.

59. Katoh, K., and Toh, H. (2008). Recent developments in the MAFFT multiple sequence alignment program. Brief. Bioinform. *9*, 286-298.

60. Maddison, D., and Maddison, W. (2000). MacClade 4: Analysis of Phylogeny and Character Evolution, (Sunderland, MA: Sinauer Associates, Inc., Publishers).

61. Felsenstein, J. (2013). PHYLIP (Phylogeny Inference Package) version 3.695. (Seattle.: Distributed by the author. Department of Genome Sciences, University of Washington.).

62. Felsenstein, J. (1985). Confidence limits on phylogenies - an approach using the bootstrap. Evolution *39*, 783-791.

63. Zhang, Y., Gu, L., Hou, Y., Wang, L., Deng, X., Hang, R., Chen, D., Zhang, X., Zhang, Y., Liu, C., and Cao, X. (2015). Integrative genome-wide analysis reveals HLP1, a novel RNA-binding protein, regulates plant flowering by targeting alternative polyadenylation. Cell Res. *25*, 864-876.

64. Licatalosi, D.D., Mele, A., Fak, J.J., Ule, J., Kayikci, M., Chi, S.W., Clark, T.A., Schweitzer, A.C., Blume, J.E., Wang, X., Darnell, J.C., and Darnell, R.B. (2008). HITS-CLIP yields genome-wide insights into brain alternative RNA processing. Nature *456*, 464-469.

65. Marchler-Bauer, A., Derbyshire, M.K., Gonzales, N.R., Lu, S., Chitsaz, F., Geer, L.Y., Geer, R.C., He, J., Gwadz, M., Hurwitz, D.I., Lanczycki, C.J., Lu, F., Marchler, G.H., Song, J.S., Thanki, N., Wang, Z., Yamashita, R.A., Zhang, D., Zheng, C., and Bryant, S.H. (2015). CDD: NCBI's conserved domain database. Nucleic Acids Res. *43*, D222-226.

66. Okano, Y., Aono, N., Hiwatashi, Y., Murata, T., Nishiyama, T., Ishikawa, T., Kubo, M., and Hasebe, M. (2009). A polycomb repressive complex 2 gene regulates apogamy and gives evolutionary insights into early land plant evolution. Proc. Natl. Acad. Sci. USA *106*, 16321-16326.

67. Stamatakis, A. (2014). RAxML version 8: a tool for phylogenetic analysis and post-analysis of large phylogenies. Bioinformatics *30*, 1312-1313.

68. Shyh-Chang, N., and Daley, G.Q. (2013). Lin28: Primal Regulator of Growth and Metabolism in Stem Cells. Cell stem cell *12*, 395-406.

69. Xu, B., Zhang, K., and Huang, Y. (2009). Lin28 modulates cell growth and associates with a subset of cell cycle regulator mRNAs in mouse embryonic stem cells. RNA *15*, 357-361.

70. Welsh, D.K., and Kay, S.A. (2005). Bioluminescence imaging in living organisms. Curr. Opin. Biotechnol. *16*, 73-78.

71. Mayr, F., and Heinemann, U. (2013). Mechanisms of Lin28-mediated miRNA and mRNA regulation--a structural and functional perspective. Int. J. Mol. Sci. *14*, 16532-16553.

72. Coruh, C., Cho, S.H., Shahid, S., Liu, Q., Wierzbicki, A., and Axtell, M.J. (2015). Comprehensive Annotation of Physcomitrella patens Small RNA Loci Reveals That the Heterochromatic Short Interfering RNA Pathway Is Largely Conserved in Land Plants. Plant Cell *27*, 2148-2162.

73. Axtell, M.J., Snyder, J.A., and Bartel, D.P. (2007). Common functions for diverse small RNAs of land plants. Plant Cell *19*, 1750-1769.

74. Lee, H., Han, S., Kwon, C.S., and Lee, D. (2016). Biogenesis and regulation of the let-7 miRNAs and their functional implications. Protein Cell *7*, 100-113.

75. Hertel, J., Bartschat, S., Wintsche, A., Otto, C., and Stadler, P.F. (2012). Evolution of the let-7 microRNA family. RNA Biol. *9*, 231-241.

76. Zimmer, A.D., Lang, D., Buchta, K., Rombauts, S., Nishiyama, T., Hasebe, M., Van de Peer, Y., Rensing, S.A., and Reski, R. (2013). Reannotation and extended community resources for the genome of the non-seed plant *Physcomitrella patens* provide insights into the evolution of plant gene structures and functions. BMC Genom. *14*, 498.

77. Chiu, W., Niwa, Y., Zeng, W., Hirano, T., Kobayashi, H., and Sheen, J. (1996). Engineered GFP as a vital reporter in plants. Curr. Biol. *6*, 325-330.

78. Hiwatashi, Y., Obara, M., Sato, Y., Fujita, T., Murata, T., and Hasebe, M. (2008). Kinesins are indispensable for interdigitation of phragmoplast microtubules in the moss *Physcomitrella patens*. Plant Cell *20*, 3094-3106.

79. Millar, A.A., and Waterhouse, P.M. (2005). Plant and animal microRNAs: similarities and differences. Funct. Integr. Genomics *5*, 129-135.

80. Budak, H., and Akpinar, B.A. (2015). Plant miRNAs: biogenesis, organization and origins. Funct. Integr. Genomics *15*, 523-531.

81. Cuperus, J.T., Fahlgren, N., and Carrington, J.C. (2011). Evolution and functional diversification of MIRNA genes. Plant Cell *23*, 431-442.

82. Arteaga-Vazquez, M., Caballero-Perez, J., and Vielle-Calzada, J.P. (2006). A family of microRNAs present in plants and animals. Plant Cell *18*, 3355-3369.

83. Zeidler, M., Gatz, C., Hartmann, E., and Hughes, J. (1996). Tetracycline-regulated reporter gene expression in the moss *Physcomitrella patens*. Plant Mol. Biol. *30*, 199-205.

84. Zhang, W., McElroy, D., and Wu, R. (1991). Analysis of rice Act1 5' region activity in transgenic rice plants. Plant Cell *3*, 1155-1165.

85. Campbell, R.E., Tour, O., Palmer, A.E., Steinbach, P.A., Baird, G.S., Zacharias, D.A., and Tsien, R.Y. (2002). A monomeric red fluorescent protein. Proc. Natl. Acad. Sci. USA *99*, 7877-7882.

86. Dai, X., and Zhao, P.X. (2011). psRNATarget: a plant small RNA target analysis server. Nucleic Acids Res.

87. Matoulkova, E., Michalova, E., Vojtesek, B., and Hrstka, R. (2012). The role of the 3' untranslated region in post-transcriptional regulation of protein expression in mammalian cells. RNA Biol. *9*, 563-576.

88. Zimmer, A.D., Lang, D., Buchta, K., Rombauts, S., Nishiyama, T., Hasebe, M., Van de Peer, Y., Rensing, S.A., and Reski, R. (2013). Reannotation and extended community resources for the genome of the non-seed plant *Physcomitrella patens* provide insights into the evolution of plant gene structures and functions. BMC Genomics *14*, 498.

89. Sakakibara, K., Nishiyama, T., Deguchi, H., and Hasebe, M. (2008). Class 1 KNOX genes are not involved in shoot development in the moss *Physcomitrella patens* but do function in sporophyte development. Evol. Dev. *10*, 555-566.

90. Tanabe, K., Nakamura, M., Narita, M., Takahashi, K., and Yamanaka, S. (2013). Maturation, not initiation, is the major roadblock during reprogramming toward pluripotency from human fibroblasts. Proc. Natl. Acad. Sci. USA *110*, 12172-12179.

91. Kim, M.H., Sato, S., Sasaki, K., Saburi, W., Matsui, H., and Imai, R. (2013). COLD SHOCK DOMAIN PROTEIN 3 is involved in salt and drought stress tolerance in Arabidopsis. FEBS Open Bio. *3*, 438-442.

92. Fusaro, A.F., Bocca, S.N., Ramos, R.L., Barroco, R.M., Magioli, C., Jorge, V.C.,

Coutinho, T.C., Rangel-Lima, C.M., De Rycke, R., Inze, D., Engler, G., and Sachetto-Martins, G. (2007). AtGRP2, a cold-induced nucleo-cytoplasmic RNA-binding protein, has a role in flower and seed development. Planta *225*, 1339-1351.

93. Nakaminami, K., Hill, K., Perry, S.E., Sentoku, N., Long, J.A., and Karlson, D.T. (2009). Arabidopsis cold shock domain proteins: relationships to floral and silique development. J. Exp. Bot. *60*, 1047-1062.

94. Sasaki, K., Kim, M.H., and Imai, R. (2007). Arabidopsis COLD SHOCK DOMAIN PROTEIN2 is a RNA chaperone that is regulated by cold and developmental signals. Biochem. Biophys. Res. Comm. *364*, 633-638.

95. Yang, Y., and Karlson, D. (2013). AtCSP1 regulates germination timing promoted by low temperature. FEBS Letters *587*, 2186-2192.

96. Yang, Y., and Karlson, D.T. (2011). Overexpression of AtCSP4 affects late stages of embryo development in Arabidopsis. J. Exp. Bot. *62*, 2079-2091.